Citation
Le, T.D. and Pham, T.M. and Hao, H. 2020. Numerical study on the flexural performance of precast segmental concrete beams with unbonded internal steel tendons. Construction and Building Materials. 248: ARTN 118362.
http://doi.org/10.1016/j.conbuildmat.2020.118362

Numerical Study on the Flexural Performance of Precast Segmental Concrete Beams with Unbonded Internal Steel Tendons

Tan D. Le[1], Thong M. Pham[2], and Hong Hao[3]

Abstract

This study presents a numerical investigation of the flexural performance of precast segmental concrete beams (PSBs) with unbonded internal steel tendons. Numerical models developed in this study using Abaqus software capture well the responses of the PSBs reported in previous studies. This is the first time a three-dimensional numerical model is built and successfully validated against experimental results of PSBs in literature. Based on the verified numerical model, intensive simulations of performances of segmental beams with different parameters and various conditions, i.e. tension-controlled, compression-controlled and balanced sections, are carried out. Based on the numerical results, the flexural behaviour of PSBs under four-point loading is extensively discussed regarding the failure modes, joint opening, stress increment in the tendon and the stress transfer mechanism. A parametric study is also conducted and the results show that the effective prestress, prestressing steel reinforcement ratio, and span length-to-tendon depth ratio strongly affect the load-carrying capacity, ductility, tendon stress increment, joint opening and failure modes of PSBs with unbonded tendons, while the loading type, concrete strength and the number of joints show insignificant effects on the flexural performance of the structure.

Keywords: Precast segmental structures; Concrete structures; Unbonded tendons; Flexural performance; Numerical analysis; Abaqus

[1]PhD Scholar, Centre for Infrastructural Monitoring and Protection, School of Civil and Mechanical Engineering, Curtin University, Kent Street, Bentley, WA 6102, Australia. Email: tan.le1@postgrad.curtin.edu.au
[2]Research Fellow, Centre for Infrastructural Monitoring and Protection, School of Civil and Mechanical Engineering, Curtin University, Kent Street, Bentley, WA 6102, Australia, (corresponding author). Email: thong.pham@curtin.edu.au
[3]John Curtin Distinguished Professor, Centre for Infrastructural Monitoring and Protection, School of Civil and Mechanical Engineering, Curtin University, Kent Street, Bentley, WA 6102, Australia, (corresponding author). Email: hong.hao@curtin.edu.au

1 Introduction

Precast segmental prestressed concrete beams (PSBs) have been increasingly used in many bridge construction projects around the world as this type of structure provides shorter construction time and better quality control. The use of unbonded tendons and dry joints are preferred for new segmental concrete bridge constructions since they enable fast installation and easy replacement in cases of deterioration. Since the analysis and design of structures with unbonded tendons are more complex due to the lack of bonding between the tendons and surrounding concrete, the current methods for prediction of deflection and the stress increment in the prestressing steel at the ultimate stage of PSBs with unbonded tendons are questionable [1-3]. Therefore, more comprehensive investigations are required for better understanding the performance of PSBs, and developing more reliable analysis, and design of such structures.

This study presents a numerical approach to simulate the flexural behaviour of PSBs with unbonded steel tendons using ABAQUS CAE [4] commercial software. To the authors' best knowledge, this is the first time a three-dimensional numerical model is successfully developed and validated against experimental results of PSBs in the literature. The validated model is used to conduct intensive simulations of PSBs with different parameters. Based on the numerical results, influences of effective prestress, reinforcement ratio, span-to-depth ratio, concrete strength, joint number and load type on the performance of PSBs are thoroughly discussed.

2 Literature review

Even though this study focuses on the behaviour of PSBs, the effects of the investigated parameters on the performance of monolithic beams are also reviewed and discussed. In the following sections, the influences of various parameters on the structural behaviour of monolithic beams are presented first.

2.1 Effect of the span-to-depth ratios on the performance of PSBs

The effects of the span-to-depth ratios of monolithic beams, L/d_{ps}, were studied by several researchers. Harajli [5] theoretically investigated the influence of span-to-depth ratio on the stress increment of beams with unbonded internal tendons. A wide range of L/d_{ps} was studied ranging from 5 to 50. It was found that increasing L/d_{ps} significantly decreased the stress increment at the ultimate stage, where the stress increment is the change in the tendon stress under the applied load, $\Delta f_{ps} = f_{ps} - f_{pe}$. In addition, the reduction in the stress increment with the increase in L/d_{ps} is directly related to the length of a plastic region in the member. As such, beams loaded with three-point loading encountered a higher reduction in Δf_{ps} with increasing L/d_{ps} as compared to beams loaded with four-point loading because the first one had a shorter plastic region than the second one. It is noted that the plastic hinge herein refers to the compressive concrete regions at and close to the loading points. On the other hand, Harajli and Kanj [6] conducted an experimental investigation on beams with the range of L/d_{ps} between 8 and 20 and found that the load type (third-point or four-point loadings) and the L/d_{ps} ratio did not have significant effects on the stress increment at the ultimate stage, which contradicted earlier analytical studies by Harajli [5]. However, no explanations for this contradictory observation were provided by the authors. Tanchan [7] conducted a numerical investigation and found that L/d_{ps} ratio greatly affected the ultimate moment capacity of the member while only a slight effect was observed for the change in Δf_{ps}. For instance, the ultimate moment capacity decreased by 50% for both four-point and three-point loadings when L/d_{ps} increased from 10 to 45. Meanwhile, Δf_{ps} slightly decreased by 9% for four-point loading and by 1% for three-point loading as the L/d_{ps} ratio increased from 10 to 35. Those values were 18% and 2% for the case of four-point loading and three-point loading respectively when the L/d_{ps} ratio increased from 35 to 45.

Meanwhile, there have been no studies on the effect of L/d_{ps} on the structural behaviour of segmental beams. Instead, the effect of shear span-to-depth ratio, a/h, on the shear resistance capacity of the structures has been studied by several researchers. Li et al. [8] conducted an experimental study on segmental simply-supported beams prestressed with external tendons under combined shear and bending forces and found that for the beams with the same type of joints, the shear resistance of joint decreased as a/h increased. When a/h changed from 1.5 to 3.5, the shear force in the joint plane at the ultimate stage reduced respectively by 45.4% and 42.8% for epoxied and dry joints although the ultimate moment capacity increased by 22.9% and 28.8%, respectively. Similar results were observed in the tests by Li et al. [9] on segmental concrete continuous beams with external tendons as the shear span ratio is inversely proportional to the shear resistance of the structure. The shear span ratio also showed an influence on the failure mode of the specimens. For the beams with epoxied joints which failed by compression shear, the larger is the shear span ratio, the less number and sparse distribution of the shear compressive cracks are.

As can be seen from the above review that the effect of a/h on the shear behaviour of segmental beams has been reported in the literature while the effect of L/d_{ps} on the flexural behaviour of segmental beams has not been addressed yet. The understandings of this parameter on the failure mode, stress increment in the tendons, and joint opening are necessary to attain better predictions of the performance of segmental beams under flexural loading.

2.2 Influence of effective prestress on the performance of PSBs

The effective prestress in the tendons, f_{pe}, is one of the main factors that strongly affects the performance of prestressed concrete beams. In the case of monolithic beams with unbonded tendons, f_{pe} was found to affect the failure modes, crack patterns and plastic rotation capacity of the structure [10-12]. The beams with high f_{pe} behaved rather like a beam with bonded tendons, and formed a deep compression zone with considerable concrete distress, together with a number of cracks in the tension zone. On the other hand, the beams with low f_{pe} showed a quite shallow compression zone but exhibited a much greater capacity for plastic rotation before failure. The beams with low f_{pe} developed two or three widely spaced cracks and only one of which continued to widen under the applied loads. Tanchan [7] conducted a numerical analysis on beams with unbonded tendons with span-to-depth ratios L/d_{ps} varying from 10-18.5 and observed that f_{pe} slightly affected the ultimate moment capacity M_u, but significantly affected the stress increment in the tendons, Δf_{ps}. As f_{pe} increased from 827 MPa to 1241 MPa, the ultimate moment capacity increased by 10% for both four-point loading and three-point loading while Δf_{ps} decreased considerably by 35%.

The effects of f_{pe} on the behavior of PSBs were investigated in several studies [13-15]. The main conclusions can be summarized as follows: (1) f_{pe} directly impacts the joint opening load, at which the lower the f_{pe}, the lower the joint opening load; (2) f_{pe} shows no influence on the stiffness of the structure while joints are closed, but strongly affects the stiffness of the structure once the joints open, i.e. the higher the f_{pe}, the stiffer the structure; (3) the maximum deflection at failure is also affected by the prestressing force - the higher f_{pe}, the larger the deflection at failure; and (4) the increase in f_{pe} leads to the increases in the load-carrying capacity of the structure. Turmo et al. [13] also noted that a minor decrease in the prestressing level can lead to a rapid loss of safety of the structure.

It is seen from the above review that studies have been conducted to investigate the effects of f_{pe} on the segmental beams' stiffness, joint opening, strength and deflection capacity of the structure. However, it is noted that these studies were conducted on segmental beams with external tendons, no studies on segmental beams with unbonded internal tendons have been reported. Furthermore, the effects of f_{pe} on the flexural performance of segmental beams regarding failure modes, stress increment in the tendons, ultimate strength and deflection capacity for different failure modes such as tension-controlled or compression-controlled sections have not yet been reported in the previous studies, which will be addressed in this study.

2.3 Effect of amount of prestressing steel on the performance of PSBs

Amount of prestressing steel, A_{ps}, is another factor strongly affecting the strength and deflection capacity of the beams with unbonded tendons. In case of monolithic beams with unbonded tendons, it was found that as the area of prestressing steel increased, the ultimate strength capacity of the structure increased, but the deflection capacity decreased. In other words, the beam is less ductile with the increase of the area of the prestressing steel [7, 16-18]. All the beams tested by

Tao and Du [16] with low values of combined reinforcement ratio were very ductile as they underwent large deflections of 90 to 120 mm (1/47 to 1/35 of the effective span) at failure while that for beams with higher values of combined reinforcement ratio was about 40 to 50 mm (1/105 to 1/93 of effective span). Moreover, the increment of stress in the tendons was also affected by A_{ps}. When A_{ps} increased from 161 mm^2 to 742 mm^2, Δf_{ps} considerably reduced by 35% as observed in the study by Tanchan [7]. Lou et al. [17, 18] conducted a numerical study on beams prestressed with unbonded fibre-reinforced polymer (FRP) tendons and observed that the ultimate deflection decreased consistently with the increase of prestressing reinforcement ratio. Lou et al. [19] examined the tendon stress increment with the variation of prestressing reinforcement ratio and found that the tendon stress increment at the ultimate stage decreased almost linearly as the reinforcement ratio increased.

In the case of segmental beams, to the authors' best knowledge the effect of A_{ps} on the flexural performance of PSBs with unbonded tendons have not been reported yet. Instead, the effects of the use of hybrid tendons were investigated by several researchers. Yuan et al. [20] experimentally investigated the behaviour of PSBs with combined external and internal tendons under bending, in which the internal tendons were bonded to concrete. The authors concluded that the tendon ratio between the internal and external tendons had a significant effect on the strength capacity and ductility of the structure. The more internal tendons were used, the higher load-carrying capacity and better ductility the beams achieved. This phenomenon is attributed to the fact that the bonding effect helps the beams with bonded tendons better mobilize the tendon strain and the use of internal tendons discarded the second-order effect occurring in the external tendons. These effects allowed the beams with more internal bonded tendons to achieve higher load-carrying capacity and deflection capacity. Therefore, the ratio between internal and external tendon not less than 1:1 was recommended by Yuan et al. [20]. This effect of tendon ratio is also valid for the case of segmental continuous concrete beams. Li et al. [9] conducted tests on segmental continuous beams and observed that the ultimate stresses in the external tendons in beams also having internal tendons were higher than those in beams having only external tendons. Jiang et al. [21] studied simply supported segmental beams with hybrid tendons and also found that the use of hybrid tendons improved both the strength and ductility compared to beams with sole external tendons.

2.4 Effect of concrete strength on the performance of PSBs

The concrete strength, f'_c, considerably affects the ultimate strength capacity and ductility of monolithic concrete beams with unbonded tendons. Tao and Du [16] tested monolithic beams with unbonded internal tendons and found that increasing f'_c led to increasing the tendon stress increment, strength, and deflection capacity of the beams. Similar results were observed in the study by Tanchan [7]. Furthermore, when f'_c increased, beams loaded under four-point loading exhibited greater increases in the ultimate moment capacity and stress increment in the tendons compared to the beams under three-point loading. When f'_c increased from 41 MPa to 82 MPa, the ultimate moment capacity was respectively increased by 10% for three-point loading and 15% for four-point loading, and Δf_{ps} was respectively increased by 20% for three-point loading and 40% for four-point loading [7]. To the authors' best knowledge, no studies on the effects of f'_c on the flexural behaviour of segmental concrete beams with unbonded tendons have been reported in the literature.

2.5 Effect of joint's type, number, and location on the performance of PSBs

Joint type

The effect of joint type on the behaviour of segmental concrete beams has been well documented in the literature. It was found that segmental beams with epoxied joints obtained higher cracking load than beams with dry joints due to the additional tensile strength of concrete [22, 23]. Loads at the first joint opening for the dry-joined specimen were about 27% less than those of the epoxy-joined specimens [23]. Saibabu et al. [23] also found that, in terms of the flexural strength, the maximum load and failure load of dry-joined specimens were 8.6% and 16.7% less than that of the epoxy-joined specimen, respectively. In terms of the shear strength, MacGregor [22] found that the joint type had no effect on the shear strength of the segmental beams. Jiang et al. [24], however, found that dry-joined specimens exhibited a lower shear strength capacity than the epoxied-joined specimens.

Regarding the rotation capacity and ductility, MacGregor [22] found that the epoxy-joined beams showed a less rotation capacity than dry-joined beams. In the epoxy-joined beams, only a single joint or crack opened resulting in large rotations to be concentrated at a single location while several midspan joints opened causing rotations being distributed over several joints in the dry-joined beams. This redistribution of the rotations helped the dry-joined beams withstand larger cumulative rotations than epoxy-joined beams. This observation was also supported by experimental results presented in other studies [2, 3, 25]. MacGregor [22] also found that the use of epoxied joints did not provide any increase in the ductility of the segmental beams compared to the use of dry joints. This conclusion, however, is contrary to the results presented in recent studies on both simply-supported and continuous segmental beams [8, 9], where beams with epoxied joints showed greater ductility compared to beams with dry joints.

Previous studies have observed that epoxied and dry joints exhibit different failure modes [1-3, 8]. The failure of epoxied joints developed in the concrete adjacent to the segment interface. In contrast, the failure of dry joints took place at the interfaces [1, 8]. Similar observations were found in the previous studies [2, 3] when testing segmental concrete beams with either dry and epoxied joints and prestressed with CFRP tendons. The response of epoxied joints was brittle and failed in a sudden manner when the applied load reached its cracking/opening load. However, after the epoxied joints opened, i.e. cracked, it exhibited similar behaviour to the dry joints under the applied load. Both the beams with dry and cracked epoxied joints underwent various load cycles until they reached the ultimate stage [2, 3].

Joint number and joint location

The effect of the number of joints on the performance of segmental beams was examined in a limited number of studies. Jiang et al. [21] found that the beam with two joints showed smaller flexural strength than the beam with seven joints. As observed in the tests, the flexural strength of the two-joint segmental beam with hybrid tendons was 12.8% less than that of the seven-segmental beam. This is due to a high concentration of rotation and deflection at individual joints in the two-segmental beams as explained by the authors. In addition, the two-joint segmental beams exhibited less deflection than the seven-joint segmented beam. Jiang et al. [24] investigated the shear behaviour of PSBs with external tendons and found that with the increase in the number of joints, the shear strength and deflection of PSBs with external tendons increased. They observed that the stiffness of the segmental beams decreased when the number of joints increased, which caused the beam with a higher joint number to undergo larger deformation. In terms of joint's location, Li et al. [8] tested segmental beams with external tendons and found that the joint location had a significant influence on the joint bearing capacity, particularly when the load was applied to the immediate vicinity of the joints. For beams with the same joint types, the joint resistance reduced when the joint locates at or near the midspan.

It can be summarized from the above review that joint type was found to have a significant effect on the flexural and shear capacity of the segmental beam, i.e. epoxied joints increased the cracking load, ultimate flexural and shear strength of the segmental beam but limited the beam's rotation capacity. However, there is a controversy regarding the ductility as several researchers observed an increase in the beam's ductility while others did not. In terms of the number of joints, researchers found that reducing the number of joints led to a lower flexural and shear strength capacity of the segmental beam, but increasing the number of joints led to the decrease in the beam's stiffness as concluded in the study by Jiang et al. [24]. In terms of joint's location, Li et al. [8] found that the joint resistance reduced when the joint approaches the beam's midspan. This study will further investigate the effect of a number of joints on the flexural behaviour of the segmental beams with unbonded internal tendons.

2.6 Effect of load type on the performance of PSBs

Previous studies showed that type of load, i.e. three-point or four-point loadings, had an insignificant effect on the flexural behaviour of monolithic beams with unbonded tendons [6, 7]. Harajli and Kanj [6] conducted an extensive test program on concrete monolithic beams prestressed or partially prestressed with unbonded tendons. The beams were tested under three-point loading and four-point loading and the tested results showed that the type of load had an insignificant effect on the nominal flexural characteristics of the beams. Tanchan [7] carried out a numerical study on monolithic beams prestressed with unbonded internal tendons and the results revealed that the change in the type of load had a minor change in the bending moment of the beams at the ultimate stage. However, Harajli et al. [26] found that the beams under three-point loading tended to mobilize less deflection at the ultimate stage compared to beams under four-point loading because it developed smaller equivalent plastic hinge length at failure. Yuan et al. [1] tested segmental beams with external tendons and observed that both the beams subjected to four-point loading and three-point loading had the same bending moments at the onset of joint opening but the latter beam exhibited a higher bending moment at the ultimate stage compared to the former one. No studies have been done to investigate the effect of loading types on the flexural behaviour of the segmental beams, except the previous study by Yuan et al. [1]. As such, further studies are necessary to obtain sufficient data in order to be able to quantitatively predict the behaviour of the segmental beams with unbonded tendons under different loading types.

2.7 Contribution of conventional steel reinforcements

For the segmental concrete beams, the longitudinal steel bars are cut-off at the joints' locations. As such, there is theoretically no contribution of longitudinal reinforcement to the tension force of the section. This was confirmed by previous studies, which were conducted on segmental concrete beams with either steel or CFRP tendons with dry/epoxied joints [2, 3]. Similar conclusions were also reached by other studies [1, 21] and confirmed that the longitudinal reinforcement contributed little to the flexural capacity of the segmental beams.

In terms of the contribution of the transverse steel reinforcement on the behaviour of PSBs, Turmo et al. [15] studied the shear behaviour of segmental beams with external tendons and found that the shear reinforcement had a minor contribution to the shear strength of the structure. After joint opening, the shear was resisted solely by the concrete on the top fibre, which was in compression. As such, no need to provide hangover steels for the shear transfer as concluded by the authors. Similar conclusions were given in recent studies [2, 8, 21] in which it was found that stirrups contributed little to the shear capacity of the structure because it is governed by weaker sections at the joints. Meanwhile, in the case of continuous segmental beams, Li et al. [9] observed that the contribution of stirrups is large than that in simply-supported beams. The contribution of stirrups to the shear strength was 14-21% of the total shear capacity.

3 Description of Finite Element Model

This section describes the use of ABAQUS CAE [4] software to simulate the behaviour of segmental concrete beams internally prestressed with unbonded tendons. Two segmental concrete beams reported in the study of Le et al. [2] and one beam tested by Jiang et al. [21] are simulated to verify the accuracy of the numerical model. Both the two beams, BS1 and BC1 in Le et al. [2] had T-shaped section and were 400 mm in height and 3.9 m of overall length. Each beam consisted of four segments, which were made of reinforced concrete and had the length of 800 mm and 1150 mm, respectively. Two steel/CFRP tendons, which were internally unbonded to the concrete were used to join these segments (Fig. 1.) Beam S-2 in Jiang et al. [21] had also T-shaped section of 400 mm height and 3.5 m overall length. The beam consisted of two joints and was prestressed with one internal unbonded and two external steel tendons. More details of the beams' dimensions, reinforcements, and material properties are found in Le et al. [2] and Jiang et al. [21].

Three-dimensional solid finite elements are used to simulate the response of the different components of the finite element models. Eight-node linear brick, reduced integration hexahedral elements (C3D8R) are selected to model concrete elements, prestressing tendons, and supplementary elements including steel loading plates, anchor blocks and steel plates at the two ends of the beam. Two-node linear 3-D truss elements (T3D2) are selected to simulate the conventional steel reinforcements (Fig. 2).

3.1 Concrete material model

Concrete damage plasticity (CDP) model incorporated in ABAQUS CAE [4] is used to model concrete elements. The CDP model is able to capture the elastic and plastic behaviours of concrete for damage characteristics in both compression and tension. It can be applied for concrete subjected to static and cyclic loadings.

General parameters of the CDP model are given as follows [27]: dilation angle ψ, flow potential eccentricity e, and viscosity parameter μ, are equal to 30°, 0.1, and 0.001, respectively; the ratio of initial equibiaxial compressive yield stress to initial uniaxial compressive yield stress, σ_{b0}/σ_{c0} = 1.16; and the ratio of the second stress invariant on the tensile meridian to the compressive meridian, K_c = 0.667. These material parameters are also summarized and listed in Table 1.

The stress-strain curve proposed by Carreira and Chu [28] is adopted in this study for concrete under compression. The relationship is expressed as follows:

$$\sigma_c = \frac{\beta\left(\varepsilon_c/\varepsilon_c^{'}\right) f_c^{'}}{\beta - 1 + \left(\varepsilon_c/\varepsilon_c^{'}\right)^{\beta}} \tag{1}$$

where f'_c and ε'_c are the compressive concrete strength (MPa) and its corresponding strain; σ_c and ε_c are the stress and strain of concrete, respectively; β is a material parameter which depends on the shape of the stress-strain diagram. A detailed procedure to compute β is provided in Carreira and Chu [28]. It is noted that a linear stress-strain relationship is assumed up to 40% of the concrete maximum compressive strength in the ascending branch [29] as shown in Fig. 3.

Inelastic strain $\tilde{\varepsilon}_c^{in}$ in Fig. 3(a) is assigned in CDP model for the compression behaviour, $\tilde{\varepsilon}_c^{in} = \varepsilon_c - \varepsilon_{oc}^{el}$, where E_c is the concrete modulus and σ_{oc}^{el} is the concrete elastic strain in compression, $\varepsilon_{oc}^{el} = \frac{\sigma_c}{E_c}$.

The compressive damage parameter d_c is also assigned in the CDP model. Birtel and Mark [30] developed the following expression to compute d_c:

$$d_c = 1 - \frac{\sigma_c E_c^{-1}}{\varepsilon_c^{pl}\left(1/b_c - 1\right) + \sigma_c E_c^{-1}} \tag{2}$$

where ε_c^{pl} is the plastic strain, which is determined proportionally to the inelastic strain $\tilde{\varepsilon}_c^{in}$ using a constant factor b_c, i.e., $\varepsilon_c^{pl} = b_c \tilde{\varepsilon}_c^{in}$. The constant factor b_c is taken as 0.7 as proposed by Birtel and Mark [30].

The stress-strain relationship for concrete in tension is assumed to consist of a linear ascending part up to the cracking strength f_{ct} and a linear descending part to a total strain of approximately 10 times the strain at the tensile cracking ε_{ct} [29]. Similar to the concrete behaviour in compression, cracking strain $\tilde{\varepsilon}_t^{ck}$ and tensile damage parameter d_t are used in the CDP model for the concrete in tension (Fig. 3b). Cracking strain $\tilde{\varepsilon}_t^{ck}$ is computed as $\tilde{\varepsilon}_t^{ck} = \varepsilon_t - \varepsilon_{ot}^{el}$, in which $\varepsilon_{ot}^{el} = \dfrac{\sigma_t}{E_c}$, where ε_{ot}^{el} is the concrete elastic strain in tension. Tensile damage parameter d_t is calculated as follows:

$$d_t = 1 - \frac{\sigma_t E_c^{-1}}{\varepsilon_t^{pl}\left(1/b_t - 1\right) + \sigma_t E_c^{-1}} \tag{3}$$

In Eq. 3, ε_t^{pl} is the plastic tensile strain, $\varepsilon_t^{pl} = b_t \tilde{\varepsilon}_t^{ck}$ and the parameter b_t is taken as 0.1 [30].

3.2 Reinforcement material model

The stress–strain curve proposed by Devalapura and Tadros [31] is adopted in this study to model the prestressing steel as given in Eq. 4. For low-relaxation prestressing steel Grade 270, which was used in Le et al. [2] and in this study, the constants *A*, *B*, *C*, *D* are taken as 887, 27613, 112.4 and 7.36, respectively.

$$f_{ps} = \varepsilon_{ps}\left[A + \frac{B}{\left\{1 + \left(C\varepsilon_{ps}\right)^D\right\}^{1/D}}\right] \le f_{pu} \tag{4}$$

For CFRP tendons, the isotropic elastic material model is chosen to model the tendons since CFRP tendons exhibit a linear stress-strain relationship up to the failure. The failure of the CFRP tendons is considered to occur when their nominal tensile strength f_{pu} (2450 MPa) is reached or when the shear stress in the tendon obtained from the simulation exceeds its nominal shear resistance. The nominal shear strength of the CFRP tendons is 126 MPa as reported in the previous studies [2, 3].

An elastoplastic stress-strain material model is used for conventional steel reinforcements in both tension and compression [32]. The longitudinal and transverse reinforcements are embedded into the concrete elements. Details of material properties are given in Table 1.

3.3 Contact mechanism

The surface-to-surface contact model incorporated in ABAQUS CAE [4] is chosen to formulate the contacts between joint surfaces of the two adjacent segments (key-key contact), and the unbonded tendons vs the surrounding concrete (unbonded tendon-concrete contact). For the key-key contact, a friction coefficient of 0.7, which is based on previous experimental studies [33, 34], is selected to define the tangential behaviour while hard contact type is used to define the normal behaviour. The hard contact type allows surfaces to develop compression behaviour when they are in contact without penetration into each other and to separate in case of tension without tensile stress transferring through the interfacial interaction. For the unbonded tendon-concrete contact, since the friction forces between the tendon and surrounding concrete are small [35-38], they are neglected in this study to simplify the analysis. As such, frictionless is assumed between the tendon and the surrounding concrete to define the tangential behaviour and hard contact type is used for the normal behaviour. Tie constraint contact type is used to model the contacts of steel loading plates to concrete, anchor blocks to steel end-plates, and steel end-plates to concrete.

3.4 Modelling procedure

The beam model is built symmetrically with regard to the beam's longitudinal axis at the centroid of the cross-section (Fig. 2). For the concrete elements, the most critical areas occurred at joint locations where the cracking happened as observed in the experiment [2, 3]. A finer mesh with an element size of 20 mm, therefore, is applied for these areas compared to a courser mesh, with the element size of 40 mm for the other areas. The prestressing tendons and the conventional steel reinforcement are meshed with an element size of 20 mm. The remaining components including steel plates and anchors are meshed with an element size of 40 mm. It is noted that mesh convergence tests are carried out by halving the mesh size from 80 mm, 40 mm and 20 mm. The numerical results show that further reducing the mesh size under 40 mm does not considerably affect the results but requires a significantly high computation cost. Therefore, the mesh size of 20 mm close to the joints and 40 mm for other regions are used in this study. In total, the numerical model consists of 38,620 nodes and 30,013 elements including 27,093 solid elements and 2,920 truss elements.

The prestressing effects in the model are specified using Predefined Fields function provided in Abaqus (2012). The effective prestress in the tendons f_{pe} after post-tensioning is specified in the model to be equal to the values reported in the work by Le et al. [2] for the tested beams. In the experiment, the applied load was exerted by two vertical hydraulic jacks placed symmetrically at one-third span length. Numerically, this is simulated by creating two boundary conditions vertically moving downward, which are also placed symmetrically at the one-third span length of the beam as shown in Fig. 2.

3.5 Model validation

Experimental results are used to validate the numerical models in terms of the load-deflection responses and failure modes (Fig. 4). As observed in Fig. 4(a), the numerical models well capture the load-deflection responses of the tested beams by Le et al. [2]. For the case of Beams BS1 with steel tendons, the test was stopped for safety reason at a very high loading level. At that point, the applied load was 96 kN and its corresponding mid-span deflection was 89.4 mm. In the numerical model, the applied load corresponding to the deflection of 89.4 mm is 91 kN, which differs by approximately -5.7% as compared to the experimental result. In the case of Beam BC1 with CFRP tendons, the numerical model also accurately predicts the applied load at the ultimate stage P_u. P_u obtained from the numerical model is approximately 115 kN, which is about 1.8% higher than the experimental result (113 kN). It is noted that the ultimate stage of Beam BC1 is taken at a step where the shear stress obtained in the tendon exceeds its nominal shear resistance. At this step, the longitudinal tensile stress in the tendon is 1925 MPa, which has not reached its nominal tensile strength yet. Similarly, the numerical model well captures the load-deflection curve of Beam S-2 tested in the study of Jiang et al. [21], although it shows a slightly higher applied load at the ultimate stage (Fig. 4b). The ultimate load obtained from the numerical result is 234 kN, which is 7.3% higher than the experimental result.

Failure modes of the tested beams are also well captured by the numerical models. As observed in the test of Le et al. [2], both Beams BS1 and BC1 exhibited very similar concrete responses in the compression zone, i.e. concrete in the compression at the middle joint J2 crushed, whereas no damage was observed in the other joints (J1, J3). Numerical models capture the same failure modes as shown in Fig. 4(c). In Fig. 4(c), only a photo showing the failure mode of Beam BS1 is provided for brevity. In the numerical model, the concrete fails when it reaches the ultimate strain of 0.003 under compression. Yielding of steel tendons is also observed in the numerical model, which takes place before the crushing of the concrete. After that, the beam continues to deform under the applied load leading to the crushing of concrete on the top fibre when it reaches its ultimate strain as observed in the experiment. For Beam BC1, the rupture of the CFRP tendons is observed in the numerical model as also seen in the experimental test. The rupture of the CFRP tendons, which happens at the middle joint location, is due to the shear stress in the tendons generated by the applied load exceeded its nominal shear resistance. It is worth noting that the rupture of the CFRP tendons was observed in the experiment but the causes, i.e. by tensile or shear stress, were not clear. This numerical simulation has revealed that shear stress primarily causes the rupture of the tendons.

From the above discussions, it is evident that the numerical model developed in this study is reliable and capable of simulating the behaviour of segmental concrete beams prestressed with unbonded internal tendons. In the next sections, intensive simulations are conducted using the validated model in this section to investigate the behaviour of PSBs with unbonded tendons under bending.

4 Flexural behaviour of segmental beams

4.1 Load-deflection curves: compression-controlled and tension controlled sections

Based on the calibrated models, various numerical models are built to investigate the load-deflection responses of PSBs with unbonded internal tendons. The beams' cross-section and conventional steel reinforcement configuration are maintained the same as the beam shown in Fig. 2. All the beams are built with dry joints while different effective prestressing stress f_{pe}, amount of prestressing steel A_{ps}, concrete strength f'_c and span length to tendon depth ratio L/d_{ps} are investigated. All the beams are loaded under four-point loading as shown in Fig. 2.

From the numerical results, there are two types of load-deflection responses for the PSBs with unbonded internal tendons (Fig. 5a). Only the load-deflection curves of two beams are presented herein for brevity for which the curve of Beam SD25-118-069 represents a typical load-deflection curve of a beam failing in tension while the one of Beam SD25-284-02 represents a typical curve for a beam failing in compression. It is noted that Beam SD25-118-069 has the ratio of L/d_{ps} of 25, is prestressed with two 11.8-mm diameter tendons at an effective prestress ratio f_{pe}/f_{pu} of 0.69. Beam SD25-284-02 has the same beam's configuration and dimensions as of Beam SD25-118-069 except for the reinforcement ratio and effective prestress for which Beam SD25-284-02 comprises two 28.4-mm diameter tendons of f_{pe}/f_{pu} of 0.20. The load-deflection curves of these two beams are also generalized in Fig. 5(b).

In the case of a tension-controlled section, the load-deflection curve of Beam SD25-118-069 is divided into two stages distinguished by a transition zone. In the first stage from Points 1 to 3, the beam exhibits a linear relationship between the applied load and deflection. Then, the middle joint starts to open at Point 3 creating a transition zone as observed in Fig. 5(b). After that, the beam behaves nonlinearly up to failure in the second stage. The failure is due to the yielding of steel tendons starting at Point 6, which occurs before the crushing of concrete in compression zone (Point 7).

In the case of a compression-controlled section, Beam SD25-284-02 also exhibits two stages in the load-deflection curve with one inflection point. However, the failure of the beam is due to the crushing of concrete in compression (Point 7), which takes place before the yielding of tendons (Point 6) as observed in the figure. After the crushing of concrete, the beam does not show sufficient ductility but fails in a brittle manner, which is not desirable for structures from a ductility and safety viewpoint.

4.2 Joint opening and tendon stress increment

Fig. 6 shows the opening of joints under the applied load. As can be seen from Fig. 6(a) that for the beams investigated in this study all the joints open under the applied load at different opening rates. The opening concentrates in the middle joint J2 at midspan while the other joints show a much smaller magnitude of opening. The opening of joints J1 (J3) of Beam SD25-118-069 (tension-controlled beam) remains constant after the tendon yields. This phenomenon is also observed in the experimental tests by Le et al. [2] in which the two side joints J1 and J3 of Beams BS1 and BC1 almost remained at the same opening level after the tendons yielded. These two beams were under-reinforced as reported by the authors. Meanwhile, that for joint J1 (J3) of Beam SD25-284-02 gradually reduces when the concrete in the compression zone reaches its elastic limit as defined in Fig. 3(a). It can be stated at this stage that the opening level of side joints (other than middle joint) depends on the level of the prestressing reinforcement ratio. However, to draw a final conclusion on the level of opening of the side joints and how they behave under the applied loads, it requires further studies in which the effects of parameters including the number of joints, joints' locations, joint types and the location of loading points need to be investigated. The total opening of all the joints under the applied load for the two beams is shown in Fig. 6(b). As seen from the figure the shape of the applied load-opening curves are similar to the applied load-deflection curves shown in Fig. 5. The load causing joints to open in Beam SD25-118-069 is about 53% of the ultimate load and that value is about 48% for the case of Beam SD25-284-020.

The opening of the joints leads to a dramatic increase in the tendon stress as observed in Fig. 7(a). Beam SD25-118-069 shows an almost constant stress increment rate until the yielding of the tendon. In contrast, the tendon in Beam SD25-284-020 shows a higher rate in the stress increment after the concrete elastic limit is reached until the ultimate stage. It is worth mentioning that the tendon stress starts to increase at the beginning of the applied load, but with a low rate. In Beam SD25-118-069, the stress in the tendon only increases by approximately 1.3% of the effective stress f_{pe} at the onset of the joint opening, while that for the tendon in Beam SD25-284-020 is approximately 9.8%. Therefore, it can be deduced from this observation that the change in the tendon stress at the opening of the joints is significantly influenced by the amount of the prestressing steel which classifies the beam's behaviour as compression control or tension control. In other words, the contribution of steel tendons at the onset of joint opening depends on the reinforcement ratio, which draws attention during the analysis and design of this type of structure. The results from the present study revealed that for the PSBs under four-point loading the ratio f_{psYP}/ f_{pe} shows an almost linear relationship with the reinforcement ratio, where f_{psYP} is the stress in the tendons at the yield point as defined in Fig. 5b.

The relationship between the stress increment and the joint opening is plotted in Fig. 7(b). For the case of the tension-controlled beam, the stress increment shows an approximately linear relationship with joint opening up to the yielding of tendons. Meanwhile, in the case of the compression-controlled beam, this linear relationship is maintained to the point where the concrete reaches its elastic limit. After that, a highly non-linear relationship is observed between the stress increment and joint opening up to the ultimate stage. Similar behaviours are observed for the relationship between the stress increment and midspan deflection as shown in Fig. 8(b). Meanwhile, the joint opening shows an almost perfectly linear relationship to the midspan deflection up to the ultimate stage as observed in Fig. 8(a). This linear relationship is valid for both the two beams investigated.

4.3 Principle stresses contours in the beam

Fig. 9 presents the principal compressive stresses contours in Beam SD25-118-069. Only compressive stresses of absolute values higher than 1.60 MPa are shown in the figure for a better visual examination. In the initial state (Fig. 9a), most of the section's height is in compression due to the effect of prestressing, except for the top fibre which is in tension as a result of the eccentricity of the prestressing force. The inclination of the principal compressive stresses shows how the shear stresses are transferred across the web in the beam, which is clearly displayed in Fig. 9(d) for the anchorage zones. Similar observations are observed for Beam SD25-284-020 as shown in Fig. 10 (a and d). After joints open there is a shift in the neutral axis as the top fibre of the section is in compression. As can be seen clearly in Fig. 9(b) that the shear and bending moment are resisted by an arch, which is formed starting at the prestressing anchorages and developing towards the top compression zone at the midspan. Similar observations were obtained in the work of Turmo et al. [13] on segmental concrete beams prestressed with external tendons as the authors found that the compression force is resisted by a concrete arch formed across all segments. In addition, it can be seen from Fig. 9 and Fig. 10 that the portion of the arch between the two loading points is narrower than the other portions and also the arch is narrower at the joint locations. Therefore, it can be deduced that the joint reduces the depth of the neutral axis. Fig. 9(c) shows the field of principal compressive stresses at the ultimate stage, where the tendon yields in the case of Beam SD25-118-069. By comparing Fig. 9(b) and Fig. 9(c), it can be observed that the height of the compression zone of the section reduces. It means that the depth of the neutral axis reduces under the applied load as the neutral axis moves towards the top fibre. The change in the depth of the neutral axis from yield point to the ultimate stage is more significant in the case of Beam SD25-284-020 compared to that of Beam SD25-118-069 and at the ultimate stage, the neutral axis depth of Beam SD25-284-020 is greater than that of Beam SD25-118-069.

5 Parametric study

Various numerical models are built to investigate the effects of a number of parameters on the flexural performance of PSBs with dry joints and prestressed with unbonded internal steel tendons. All the beams have the same T-shape cross-section, the configuration of conventional reinforcement as shown in Fig. 1 and a ratio of L/d_{ps} of 25 except the beams in Section 5.3, where different values of L/d_{ps} are used. More details of the material properties defined in the models and beams' configuration for the parametric study are given in Tables 1-2.

5.1 Influence of effective prestress, f_{pe}

In this section, three beams with different effective prestress levels are built to investigate the effect of f_{pe} (Table 2). It is found that f_{pe} strongly affects the flexural performance of PSBs with unbonded tendons as the f_{pe} affects not only the load-carrying capacity and ductility of the segmental beams but also the failure modes of the structure. It is seen from Fig. 11(a) that increasing f_{pe} leads to increases in the opening load and maximum load of the beam. As the ratio f_{pe}/f_{pu} increases from 0.60 to 0.74 and 0.81, the opening load increases respectively by approximately 27% and 34% while the maximum load increases by 20% and 22%, respectively. It is noted that the increase in the opening load is linearly proportional to the increase in f_{pe} but this correlation does not exist for the ultimate load. This is because the failure mode of Beam SD25-190-081 differs from the failure modes of Beam SD25-190-060 and Beam SD25-190-074. Beam SD25-190-081 with only 9% of allowable strain reserved in the tendons fails in tension while the other two beams, Beam SD25-190-060 and Beam SD25-190-074, fail in compression. This brings to another conclusion that the change in f_{pe} results in the change in the failure modes of PSBs. Beam SD25-190-060 with a ratio f_{pe}/f_{pu} of 0.60 fails in compression, for which the concrete in the compression zone fails before the yielding of prestressing steel. The stress in the tendon is 1407 MPa when the top concrete crushes as can be seen from Fig. 11(b). However, when f_{pe}/f_{pu} increases from 0.60 to 0.81, the failure mode shifts to tension-controlled as observed in Beam SD25-190-081, for which the yielding of the tendon takes place before the crushing of concrete in the compression zone (Fig. 11a).

In addition, increasing f_{pe} significantly reduces the beam's deflection under the applied load. By comparing the load-deflection curves of Beam SD25-190-060 and SD25-190-074 (Fig. 11a), which have the same failure mode, it can be seen that under the same level of the applied load, Beam SD25-190-074 clearly exhibits less deflection than Beam SD25-190-060 after the opening of joints. This draws attention in the design of the structure regarding the deflection limits in the serviceability limit state. It is worth mentioning that Beam SD25-190-074 with higher f_{pe} exhibits smaller deflection at the ultimate stage as compared to that of Beam SD25-190-060. This observation is contrary to the results from previous studies [13, 14] as they found that higher f_{pe} led to larger maximum deflection at failure of the beam. An effort has been made to verify this contradiction, in which beams with different prestressing reinforcement ratios and effective prestresses are built. The results are plotted in Fig. 11(c) which clearly shows that increasing f_{pe} significantly reduces the beams' deflections at the ultimate stage. This decrease in the beams' deflections at the ultimate stage is valid for both the beams failing in compression and tension. As can be seen in the figure, Beam SD25-284-01 which fails in compression deforms 132 mm at the ultimate stage, while those for Beams SD25-284-02 and SD25-284-03 are 102 mm and 86 mm, respectively. In the case of tension-controlled failures, Beam SD25-134-063 undergoes 160 mm deflection at the ultimate stage, i.e. when tendon yields while that for Beam SD25-134-083 is 47 mm. The higher the f_{pe}, the less the workable stress reserved in the tendon. This less stress reservation in the tendon explains the decrease in the beam's deflection at the ultimate stage as observed in the beams showed in Fig. 11 (a and c).

5.2 Effect of amount of prestressing steel, A_{ps}

Three beams with different prestressing reinforcement ratios are considered in this section in order to investigate the effect of A_{ps} on the flexural behaviour of PSBs. All the beams have the same f_{pe}/f_{pu} ratio of 0.6 (Table 2). It is seen from Fig. 12(a) that the change in A_{ps} leads to the change in the beam's failure modes. Beam SD25-190-06 which is prestressed with two 190-mm diameter tendons fails in a compression-controlled manner. However, the failure mode shifts to tension-controlled when the beam is prestressed with two 134-mm tendons as observed in Beam SD25-134-06.

The change in A_{ps} also affects the load-carrying capacity and stress increment in the tendons. As observed in Fig. 12, increasing A_{ps} results in an increase in the opening load and maximum load-carrying capacity of the beam but decreases the stress increment in the tendon at the ultimate stage. When the reinforcement ratio increases from 0.14% (Beam SD25-134-06) to 0.28% (Beam SD25-190-06), the maximum load increases by 92% while the stress increment decreases by 44%. Since the stress increment in the tendon is generated by the deformation of the beam and it shows to be linearly related to the deflection of the beam as seen in Fig. 8(b), this reduction in the tendon stress increment explains the reduction in the deflection capacity of the beam when A_{ps} increases. As observed in Fig. 12(a), Beam SD25-134-060 deforms approximately 160 mm at the ultimate stage while those for Beam SD25-152-060 and SD25-190-060 are 118 mm and 85 mm, respectively. Similar conclusions were made from previous studies on monolithic beams with internal unbonded tendons [7, 16] as the area of prestressing steel increased, the ultimate strength capacity of the structure increased, but the deflection capacity decreased.

The prestressing reinforcement ratio also affects the stress increment at the opening of the joints. The yield point (as defined in Fig. 5b) is adopted in this study to represent the transition between the first stage of behaviour when the joints still close and the second stage when the joints open. Various numerical models with different values of f_{pe} and A_{ps} are built, in which f_{pe}/f_{pu} varies from 0.1 to 0.81 and ρ_{ps} varies from 0.10% to 0.64%. The concrete compressive stresses in the bottom fibre at the midspan, σ_c, due to f_{pe} are measured, which are in between 5.49 MPa and 29.80 MPa (σ_c/f'_c = 0.12 to 0.68). The relationship between the stress in the tendon at the yield point, f_{psYP} and the prestressing reinforcement ratio, ρ_{ps} is plotted in Fig. 12(c). It is seen from the figure that there is an almost linear relationship between the ratio f_{psYP}/ f_{pe} and the prestressing reinforcement ratio. In other words, increasing A_{ps} leads to an increase in the tendon stress increment at the yield point.

As observed in Fig. 12(c), when the prestressing reinforcement ratio is 0.14%, the stress increment in the tendon at the yield point is only about 2%. But, when the prestressing reinforcement ratio increases to 0.64%, an increase of about 12% is observed in the tendon stress. This observation deserves attention during the analysis and design of the structure for the calculation of cracking load, which is required for the calculation of the beam's deflection. Existing design codes [39-41] recommend the use of the effective prestress f_{pe} for the calculation of the cracking load for the stress increment in the tendon at the cracking is small. However, it can be seen from this study that the stress increment in the tendon at cracking/opening is considerably larger than the effective prestress f_{pe} and the increment is related to the prestressing reinforcement ratio as observed in Fig. 12(c). Therefore, the increase in the tendon stress at the yield point should be taken into consideration during the calculation of the cracking/opening load in order to yield a better prediction of the beam's deflection.

5.3 Effect of span-to-depth ratio, L/d_{ps}

Three beams with L/d_{ps} of 25, 35, and 45 are considered in this section to study the effect of L/d_{ps} on the flexural capacity of PSBs. These three beams have the same cross-section, effective depth of the tendons and materials' properties except for the span length. More beams' details are given in Table 2. It is seen from Fig. 13 that increasing L/d_{ps} ratio significantly reduces the load-carrying capacity of the beam at the yield point and at the ultimate stage. When L/d_{ps} increases from 25 to 35 and 45, the yielding load decreases by 38% and 65% and the maximum load decreases by 36% and 63%, respectively.

L/d_{ps} significantly affects the stress increment in the tendon. The tendon stress at the ultimate stage respectively decreases by 10% and 22% as L/d_{ps} increases from 25 to 35 and 45. This observation is similar to the findings by Harajli [5] on monolithic beams with internal unbonded tendons, however, it differs from the results obtained by Tanchan [7] and Harajli and Kanj [6]. Tanchan [7] and Harajli and Kanj [6] also conducted researches on monolithic beams with internal unbonded tendons and found that the change of L/d_{ps} did not lead to a significant change in the tendon stress increment. This study also found that the tendon stress at the yield point shows an almost linear relationship with L/d_{ps} ratio as shown in Fig. 13(c). As L/d_{ps} ratio increases the tendon stress at the yield point decreases and the level of this decrease is greater for the beams with higher prestressing reinforcement ratios.

5.4 Effect of load type

Two beams are built to investigate the effect of load type on the flexural behavior of PSBs with unbonded tendons. The two beams have the ratio L/d_{ps} of 25, internally prestressed with two 28.4-mm diameter tendons at the effective prestress of f_{pe}/f_{pu} of 0.3. One beam is loaded under there-point loading at the midspan and the other under four-point loading placed symmetrically at one-third of the span. Fig. 14 shows the deflection and stress increment in the tendon of the two beams under the applied load. It is seen from the figure that the type of load has a minor effect on the flexural behaviour of the beams investigated in this study. Although the beam under three-point loading exhibits lower deflection and the stress increment in the tendon at the yield point (when joints opened as defined in Fig. 5b), both the beams achieve almost the same bending moments, deflections and stress increments at the ultimate stage as shown in the figure. The bending moment, deflection and the tendon stress increment of Beam SD25-284-4P are respectively 278 kN.m, 86.6 mm, and 252 MPa while those values of Beam SD25-284-3P are 276 kNm, 95.2 mm, and 264 MPa, respectively. Yuan et al. [1] also observed a reduction in the deflection and stress increment of the beam loaded under three-point loading, however, this beam showed a bending moment at the ultimate stage about 17% greater than the beam under four-point loading. It is worth mentioning that changing the load type also affects the distance between the loading points to the nearest joints, which shows a significant influence on the beam performance. Therefore, the effect of load type in segmental beams is scenario-dependent and is associated with the influence of the distance between the loading point and the nearest joint.

5.5 Effect of concrete strength and number of joints

Three beams with different compressive concrete strengths are considered in this section. All the beams are prestressed with two 28.4-mm diameter tendons at the prestressing level f_{pe}/f_{pu} of 0.2 (Table 2). It is seen from Fig. 15 that the variation in the concrete strength does not lead to a considerable change in the beam's strength and ductility. All the three beams fail by crushing of concrete in the compression zone in the top fibre. When f_c' increases from 34 MPa to 54 MPa, the maximum load of the beam only increases by approximately 3%. Similarly, all the beams exhibit insignificant differences in the tendon stresses at the corresponding maximum load. This increment is small as compared to the results of the monolithic beams where the previous studies found that the maximum loads increased with the increase in the concrete strength [7]. Tanchan [7] used high-strength concrete; when the concrete strength was doubled from 41 MPa to 82 MPa a 15% increase in the ultimate load of the beam under four-point loading was achieved. In this study, the ultimate load of the segmental beam increased by 3% when the concrete strength increased by 59%. In terms of beam's stiffness, the beam with higher concrete strength exhibits slightly higher initial stiffness, which results in a slightly higher yield load. The applied load at yield point of Beam SD25-284-C54 is 42.7 kN, which is approximately 9% higher than that of Beam SD25-284-C34 which is 39.1 kN.

Beams with different numbers of joints, i.e. 3, 5 and 9 joints, are built to study the effect of the number of joints on the flexural performance of PSBs with unbonded tendons. All the specimens are loaded under four-point loading. As observed in Fig. 16, the number of joints has no effect on the behaviour of the structure under bending. All the specimens exhibit almost the same load-deflection responses and the stress increment in the tendon under the applied loads. This is attributed to the fact that with the same type of load and L/d_{ps} ratio, the stiffness and the strength capacity of the beam depend only on the cross-section properties. This explains the same load-carrying capacity and deflection capacity of the beams obtained from the numerical results. However, this finding differs from the experimental results in previous studies [21, 24] where the increase in the number of joints led to the decrease in the structure's stiffness, which in turn caused the beam to undergo larger deflections under the same level of the applied load. However, no explanations or figures to clarify this reduction in the beams' stiffness were provided in their works. The contact between joint surfaces might be the reason for this difference. In the experimental work, it is nearly impossible to obtain a perfect contact condition between the joints' surfaces. As such, the more joints the beam had, the larger contact errors accumulated in the beam. These imperfect contacts might lead to the reduction in the area of concrete of the cross-section in the compression zone, which resulted in the reduction in the beam's stiffness. In contrast, perfect contact condition between the segment joints is obtained in the numerical models which, therefore, disregards the contact errors in the simulation. It, however, requires further experimental and numerical works to confirm this observation on the effect of the number of joints on the stiffness of the segmental concrete beams.

6 Discussion on the accuracy of the analytical predictions

The accuracy of existing models for predicting the ultimate stress in the unbonded tendons of PSBs is evaluated in this section. The examined models include equations for predicting f_{ps} recommended by AASHTO LRFD [40], ACI 318 [41] and Naaman and Alkhairi [42]. Various PSB models are considered. The effects of four main parameters on the strength capacity of PSBs under four-point bending are analysed. These include the ratio of span length to tendon depth L/d_{ps}, the effective prestressing stress f_{pe}, the area of prestressing tendons A_{ps}, and the concrete strength f'_c. All the considered specimens have the same section geometry as shown in Fig. 1. Table 3 gives details of the beams' configuration.

6.1 Existing models for prediction of fps

AASHTO LRFD [40] recommended the following equation to predict the stress in the unbonded tendons of PSBs:

$$f_{ps} = f_{pe} + 6200\left(\frac{d_{ps} - c}{l_e}\right), MPa \tag{5}$$

where f_{pe} is the effective tensile stress of the tendons, $l_e = L/(1+[N/2])$, in which L is the length of the tendon between anchorages, and N is the number of support hinges crossed by the tendon between anchorages. For a simply supported beam, l_e is equal to the span length L.

ACI 318 [41] adopted the following expression for the computation of f_{ps}:

$$f_{ps} = f_{pe} + 69 + \frac{f_c^{'}}{100\rho_{ps}}, MPa \tag{6}$$

where ρ_{ps} is the prestressing reinforcement ratio. This equation is applicable to beams with $L/d_{ps} \leq 35$ as recommended by the code.

Naaman and Alkhairi [42] proposed the following equation to predict the stress in the unbonded tendons at the ultimate stage:

$$f_{ps} = f_{pe} + \Omega_u E_{ps} \varepsilon_{cu}\left(\frac{d_{ps}}{c_u} - 1\right) \tag{7}$$

where E_{ps} is the tendon modulus of elasticity, ε_{cu} is the ultimate concrete compression strain which is taken as 0.003; and Ω_u is a strain reduction coefficient. For conservative predictions, Naaman and Alkhairi [42] recommended $\Omega_u = 3.0/(L/d_{ps})$ for uniform or four-point loading, where L is the span length.

6.2 Comparisons with numerical results

It can be seen from Fig. 17 (a and b) that the two examined codes yield relatively good predictions of tendon stress, f_{ps} at the ultimate stage. All the predicted results are conservative as they are smaller than the corresponding numerical results. However, AASHTO LRFD [40]'s equation yields better predictions than those of ACI 318 [41]. The mean value of the ratio of the predicted to simulated f_{ps} by AASHTO LRFD [40] is 0.82 with the corresponding SD of 0.14 while those values for ACI 318 [41] are 0.71 with SD of 0.12, respectively. All the codes show consistent trends in the change of f_{ps} with respects to the change of the studied parameters, including L/d_{ps}, f_{pe}, and f'_c, but do not capture well f_{ps} when A_{ps} varies. As a consequence, AASHTO LRFD [40]'s model gives more accurate predictions of P_u at the ultimate stage compared to ACI 318 [41]'s model (Fig. 18a,b). The mean value of the predicted to simulated results of P_u is 0.84 with SD of 0.13, while those values for ACI 318 [41] are 0.75 with SD of 0.08, respectively. All the two codes give conservative predictions of P_u for all the beams, except for the case of Beam SD11-284-03, where AASHTO LRFD [40]'s model slightly over-predicts P_u by about 7% compared to numerical results. It is noted that Specimen SD11-284-03 has the ratio of L/d_{ps} equal to 11, which is the shortest span length considered in this study.

Meanwhile, Naaman and Alkhairi [42]'s model captures very well the changes of f_{ps} in respect to the changes of all the investigated parameters (Fig. 17c). However, it overestimates f_{ps} at the ultimate stage. The mean value of the ratio between the predicted and simulated results of f_{ps} is 1.04 with SD of 0.09 (Fig. 17c). As a result, the model over-estimates P_u at the ultimate stage as shown in Fig. 19(c). The mean value of the ratio between the predicted and simulated results of P_u is 1.06 with SD of 0.09. It is worth noting that the value of the strain reduction factor $\Omega_u = 3.0/(L/d_{ps})$ is used in this analysis, which was recommended by Naaman and Alkhairi [42] for code purposes for conservative predictions of f_{ps}. In fact, Naaman and Alkhairi [42] found that $\Omega_u = 5.4/(L/d_{ps})$ show the best correlation between the experimental and analytical results for the case of monolithic beams with unbonded tendons. Segmental beams with dry joints, however, are used in this study that explain the over-estimation of f_{ps}, hence P_u at the ultimate stage as observed.

It is, therefore, suggested to use the numerical results to determine the value of Ω_u which will lead to a better correlation between the numerical results and predicted values of f_{ps}. Four main parameters are focused in this study and are presented in Table 3. These parameters are: (1) span length to tendon depth L/d_{ps} ratio which ranges from 11 to 45; (2) area of prestressing tendons A_{ps} and (3) the effective prestress, in which they vary in a range to generate compressive concrete stress in the section after prestressing between $0.16f'_c$ and $0.54f'_c$; and (4) concrete strength f'_c of 34 MPa, 44 MPa, and 54 MPa. All the beams are subjected to four-point loading. The value $\Omega_u = 2.4/(L/d_{ps})$ leads to the best correlation between the numerical and analytical results for f_{ps}, Δf_{ps}, *and* P_u as shown in Fig. 19. All the mean values of the predicted to simulated results and their SD values are greatly improved as seen in the figure.

7 Conclusion

The numerical models developed in this study using Abaqus software capture well the responses of the segmental concrete beams reported in the literature. The verified numerical models are used to conduct intensive simulations of behaviour of segmental beams with different parameters for tension-controlled, compression-controlled and balanced sections. Flexural behaviour of PSBs with unbonded tendons in terms of failure modes, joint opening and stress increment in the prestressing tendons are discussed.

It is found from the parametric study that effective prestress in the tendon strongly affects the load-carrying capacity, deflection and failure modes of concrete segmental beams. Beams with higher effective prestress exhibit greater load-carrying capacity but less deflection at the ultimate stage. With the same prestressing amount, the change in effective prestress can lead to the change in the failure modes from compression- or tension-controlled failures.

Increasing the prestressing reinforcement ratio leads to the increase in the load-carrying capacity of the segmental beams, but decreases the beam's deflection. The stress increment in the tendon at the cracking/opening of the joint is found to be considerable in this study however it is not considered in the current design codes. 2% to 12% increase in the tendon stress at the cracking/opening is observed in this study and this stress increment is directly related to the area of prestressing steel.

Increasing the span-to-depth ratio significantly reduces the load-carrying capacity of the beam and stress increment in the tendon, and the level of decrease in the tendon stress incensement is greater in the beam with a higher reinforcement ratio.

The load type has an insignificant effect on the flexural behaviour of the beam, although the beam loaded with three-point loading registers lower deflection and stress increment in the tendon at the yield point of the structure compared to the beam loaded under four-point loading.

The concrete strength and number of joints show insignificant effects on the flexural performance of the segmental beams in terms of the load-carrying capacity, deflection and failure mode.

Finally, the accuracy of existing predictive models is examined, it is found that Naaman and Alkhairi [42]'s model yields the most closest predictions of the strength of PSBs with unbonded steel tendons at the ultimate stage. The model captures very well the changes of f_{ps} with respects to the changes of all the studied parameters. However, it overestimates f_{ps}, hence P_u at the ultimate stage. Based on the numerical results, a new value of Ω_u was suggested for better predictions of strength of PSBs with unbonded steel tendons.

Acknowledgements

The authors acknowledge the financial support from the Australian Research Council Laureate Fellowships FL180100196. The first author would also like to thank Hong Duc University, Thanh Hoa, Vietnam for the support during his study course.

References

[1] Yuan A, He Y, Dai H, Cheng L. Experimental Study of Precast Segmental Bridge Box Girders with External Unbonded and Internal Bonded Posttensioning under Monotonic Vertical Loading. J. Bridge Eng. 2014;20(4):04014075.

[2] Le TD, Pham TM, Hao H, Hao Y. Flexural behaviour of precast segmental concrete beams internally prestressed with unbonded CFRP tendons under four-point loading. Eng. Struct. 2018;168(2018):371-83.

[3] Le TD, Pham TM, Hao H, Yuan C. Performance of precast segmental concrete beams posttensioned with carbon fiber-reinforced polymer (CFRP) tendons. Compos. Struct. 2019;208:56-69.

[4] ABAQUS CAE. Analysis user's manual, Version 6.12: ABAQUS; 2012.

[5] Harajli MH. Effect of span-depth ratio on the ultimate steel stress in unbonded prestressed concrete members. ACI Struct. J. 1990;87(3):305-12.

[6] Harajli MH, Kanj MY. Service Load Behavior of Concrete Members Prestressed with Unbonded Tendons. J. Struct. Eng. 1992;118(9):2569-89.

[7] Tanchan P. Flexural behavior of high-strength concrete beams prestressed with unbonded tendons: Rutgers University; 2003.

[8] Li G, Yang D, Lei Y. Combined shear and bending behavior of joints in precast concrete segmental beams with external tendons. J. Bridge Eng. 2013;18(10):1042-52.

[9] Li G, Zhang C, Niu C. Experimental study on shear behavior in negative moment regions of segmental externally prestressed concrete continuous beams. J. Bridge Eng. 2013;18(4):328-38.

[10] Tam A, Pannell F. The ultimate moment of resistance of unbonded partially prestressed reinforced concrete beams. Mag. Concr. Res. 1976;28(97):203-8.

[11] Pannell F. The ultimate moment of resistance of unbonded prestressed concrete beams. Mag. Concr. Res. 1969;21(66):43-54.

[12] Tan K-H, Ng C-K. Effects of deviators and tendon configuration on behavior of externally prestressed beams. ACI Struct. J. 1997;94(1):13-22.

[13] Turmo J, Ramos G, Aparicio AC. FEM study on the structural behaviour of segmental concrete bridges with unbonded prestressing and dry joints: Simply supported bridges. Eng. Struct. 2005;27(11):1652-61.

[14] Turmo J, Ramos G, Aparicio AC. FEM modelling of unbonded post-tensioned segmental beams with dry joints. Eng. Struct. 2006;28(13):1852-63.

[15] Turmo J, Ramos G, Aparicio ÁC. Shear behavior of unbonded post-tensioned segmental beams with dry joints. ACI Struct. J. 2006;103(3):409-17.

[16] Tao X, Du G. Ultimate stress of unbonded tendons in partially prestressed concrete beams. PCI J. 1985;30(6):72-91.

[17] Lou T, Liu M, Lopes SMR, Lopes AV. Effect of bond on flexure of concrete beams prestressed with FRP tendons. Compos. Struct. 2017;173:168-76.

[18] Lou T, Lopes SMR, Lopes AV. Numerical analysis of behaviour of concrete beams with external FRP tendons. Constr. Build. Mater. 2012;35:970-8.

[19] Lou T, Lopes SM, Lopes AV. Response of continuous concrete beams internally prestressed with unbonded FRP and steel tendons. Compos. Struct. 2016;154(2016):92-105.

[20] Yuan A, Dai H, Sun D, Cai J. Behaviors of segmental concrete box beams with internal tendons and external tendons under bending. Eng. Struct. 2013;48:623-34.

[21] Jiang H, Cao Q, Liu A, Wang T, Qiu Y. Flexural behavior of precast concrete segmental beams with hybrid tendons and dry joints. Constr. Build. Mater. 2016;110:1-7.

[22] MacGregor RJG. Evaluation of strength and ductility of a three-span externally post-tensioned box girder bridge model: University of Texas at Austin; 1989.

[23] Saibabu S, Srinivas V, Sasmal S, Lakshmanan N, Iyer NR. Performance evaluation of dry and epoxy jointed segmental prestressed box girders under monotonic and cyclic loading. Constr. Build. Mater. 2013;38:931-40.

[24] Jiang H, Li Y, Liu A, Ma ZJ, Chen L, Chen Y. Shear Behavior of Precast Concrete Segmental Beams with External Tendons. J. Bridge Eng. 2018;23(8):04018049.

[25] Pham TM, Le TD, Hao H. Behaviour of Precast Segmental Concrete Beams Prestressed with CFRP Tendons. Proc., 9th International Conference on Fibre-Reinforced Polymer (FRP)

Composites in Civil Engineering (CICE 2018) 2018:945-53.

[26] Harajli M, Khairallah N, Nassif H. Externally prestressed members: evaluation of second-order effects. J. Struct. Eng. 1999;125(10):1151-61.

[27] Yapar O, Basu PK, Nordendale N. Accurate finite element modeling of pretensioned prestressed concrete beams. Eng. Struct. 2015;101(2015):163-78.

[28] Carreira DJ, Chu K-H. Stress-strain relationship for plain concrete in compression. J. Proc. 1985;82(6):797-804.

[29] Shamass R, Zhou X, Alfano G. Finite-Element Analysis of Shear-Off Failure of Keyed Dry Joints in Precast Concrete Segmental Bridges. J. Bridge Eng. 2014;20(6):04014084.

[30] Birtel V, Mark P. Parameterised finite element modelling of RC beam shear failure. ABAQUS Users' Conf.2006. p. 95-108.

[31] Devalapura RK, Tadros MK. Stress-strain modeling of 270 ksi low-relaxation prestressing strands. PCI J. 1992;37(2):100-5.

[32] Xu X, Liu Y, He J. Study on mechanical behavior of rubber-sleeved studs for steel and concrete composite structures. Constr. Build. Mater. 2014;53:533-46.

[33] Buyukozturk O, Bakhoum MM, Michael Beattie S. Shear behavior of joints in precast concrete segmental bridges. J. Struct. Eng. 1990;116(12):3380-401.

[34] Zhou X, Mickleborough N, Li Z. Shear strength of joints in precast concrete segmental bridges. ACI Struct. J. 2005;102(1):3.

[35] Ellobody E, Bailey CG. Behaviour of unbonded post-tensioned one-way concrete slabs. Adv. Struct. Eng. 2008;11(1):107-20.

[36] Lou T, Lopes SMR, Lopes AV. Nonlinear and time-dependent analysis of continuous unbonded prestressed concrete beams. Computers & Structures 2013;119:166-76.

[37] Knight D, Visintin P, Oehlers D, Ali MM. Simulating RC beams with unbonded FRP and steel prestressing tendons. Compos. B Eng. 2014;60:392-9.

[38] El Meski F, Harajli M. Evaluation of the flexural response of CFRP-strengthened unbonded posttensioned members. J. Compos. Constr. 2014;19(3):04014052.

[39] PCI. Design Handbook. Chicago, IL: 6th ed., Precast/Prestressed Concrete Institute; 2004.

[40] AASHTO LRFD. Bridge Design Specifications, 8th Edition (LRFD-8). Washington, DC: American Association of State Highway and Transportation Officials; 2017.

[41] ACI 318. Building Code Requirements for Structural Concrete and Commentary (ACI 318-19). Farmington Hills, MI: American Concrete Institute; 2019.

[42] Naaman AE, Alkhairi F. Stress at ultimate in unbonded prestressing tendons: Part 2—Proposed Methodology. ACI Struct. J. 1991;88(6):683-92.

List of figures

Fig. 1. Detailed dimensions of the tested beams in Le et al. [2]

Fig. 2. Components of the finite element models: Symmetricity along beam’s cross-section

Fig. 3. CDP model for concrete

Fig. 4. Numerical vs experiment results

Fig. 5. Load-deflection curves

Fig. 6. Load vs joint opening curves (refer to Fig. 2 for joints’ locations)

Fig. 7. Relations between applied load, stress increment and joint opening

Fig. 8. Relations between joint opening, deflection and stress increment

Fig. 9. Beam SD25-118-069: principal compressive stress distributions

Fig. 10. Beam SD25-284-020: principal compressive stress distributions

Fig. 11. Effect of f_{pe}

Fig. 12. Effect of A_{ps}

Fig. 13. Effect of L/d_{ps}

Fig. 14. Effect of load type

Fig. 15. Effect of f'_c

Fig. 16. Effect of number of joints

List of tables

Table 1. Details material properties used in Le et al. [2] and in this study

Table 2. Beams’ configuration for parametric study

Table 3. Beams’ configuration for strength evaluation

List of Tables

Table 1

Details material properties used in Le et al. [2] and in this study.

Concrete			CDP Parameters	
			ψ	30°
Compressive strength (MPa)	44		e	0.1
Tensile strength (MPa)	2.65		σ_{b0}/σ_{c0}	1.16
Elastic modulus E_c (GPa)	31.17		K_c	0.667
Poisson's ratio	0.18		μ	0.001
Steel Reinforcement				
	∅12	∅10	Steel tendons	CFRP tendons
Area (mm^2)	113	78.5	78.5	126.7
Elastic modulus E_s (GPa)	200	200	195	145
Yielding stress (MPa)	534	489	1674	-
Ultimate stress (MPa)	587	538	1860	2450
Poisson's ratio	0.3	0.3	0.3	0.27

Table 2

Beams' configuration for parametric study.

Group	Specimen	f_{pe}/f_{pu}	ρ_{ps}	L/d_{ps}	f'_c	No. of joints	Load type
1	SD25-190-060	0.60					
(f_{pe})	SD25-190-074	0.74	0.64%	25	44	3	four-point loading
	SD25-190-081	0.81					
2	SD25-190-060		0.28%				
(A_{ps})	SD25-152-060	0.6	0.18%	25	44	3	four-point loading
	SD25-134-060		0.14%				
3	SD25-284-030			25			
(L/d_{ps})	SD35-284-030	0.3	0.64%	35	44	3	four-point loading
	SD45-284-030			45			
4	SD25-284-C34				34		
(f'_c)	SD25-284-C44	0.2	0.64%	25	44	3	four-point loading
	SD25-284-C54				54		
5	SD25-284-3J					3	
(No. of joints)	SD25-284-5J	0.3	0.64%	25	44	5	four-point loading
	SD25-284-9J					9	
6	SD25-284-4P	0.3	0.64%	25	44	3	four-point loading
(Load type)	SD25-284-3P						three-point loading

Table 3
Beams' configuration for strength evaluation

Group	Specimen	L/d_{ps}	f_{pe}/ f_{pu}	ρ_{ps}	f'_c
1	SD11-284-03	11			
(L/d_{ps})	SD15-284-03	15			
	SD25-284-03	25	0.3	0.64%	44
	SD35-284-03	35			
	SD45-284-03	45			
2	SD25-284-01		0.1		
(f_{pe})	SD25-284-02	25	0.2	0.64%	44
	SD25-284-03		0.3		
3	SD25-284-03			0.64%	
(A_{ps})	SD25-190-03	25	0.3	0.28%	44
	SD25-152-03			0.18%	
4	SD25-284-C34				34
(f'_c)	SD25-284-C44	25	0.2	0.64%	44
	SD25-284-C54				54

List of figures

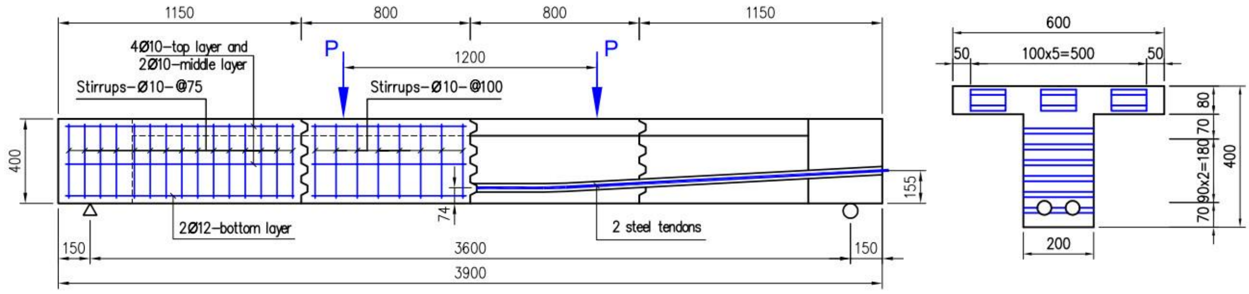

Fig. 1. Detailed dimensions of the tested beams in Le et al. [2]

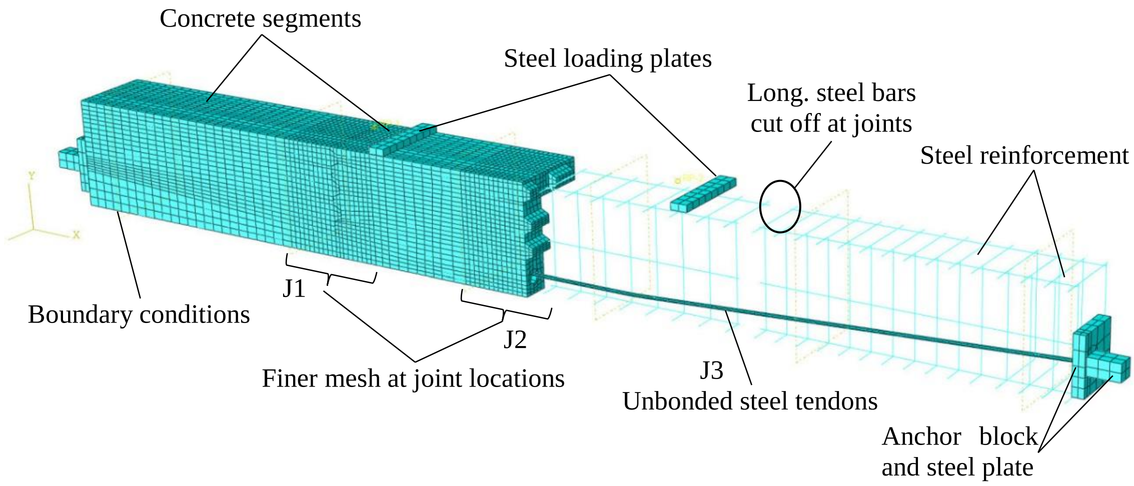

Fig. 2. Components of the finite element models: Symmetricity along beam's cross-section

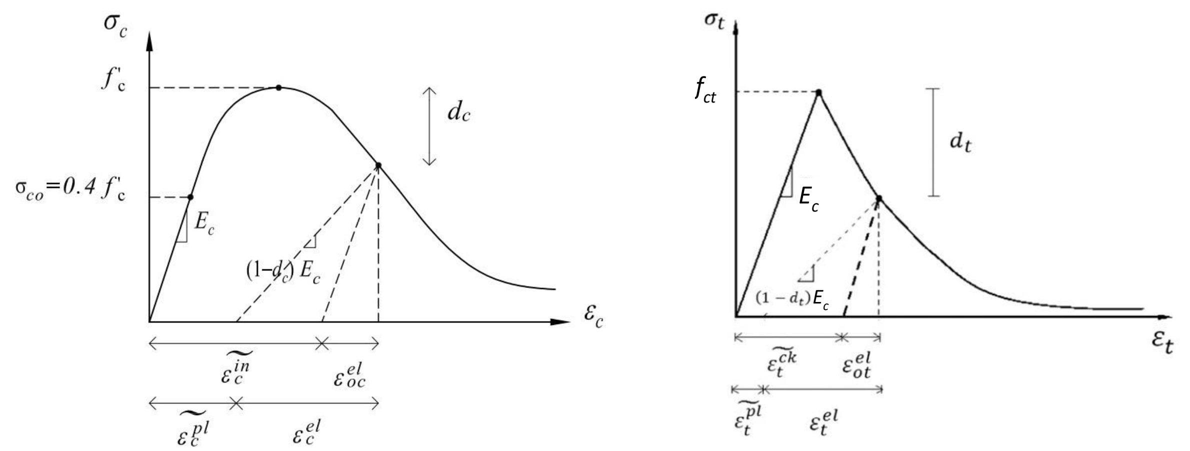

(a) Compression behavior (b) Tension behavior

Fig. 3. CDP model for concrete (Abaqus 2012)

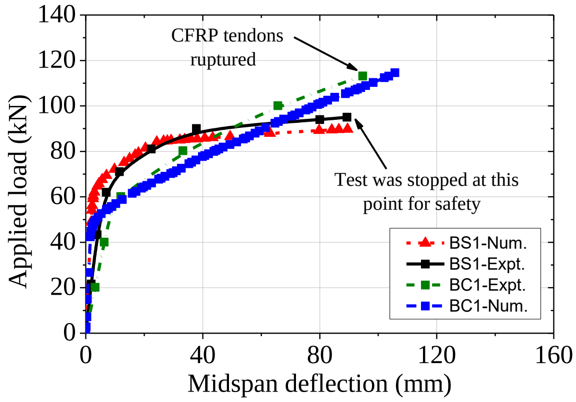

(a) PSBs with steel and CFRP tendons (Le et al. [2])

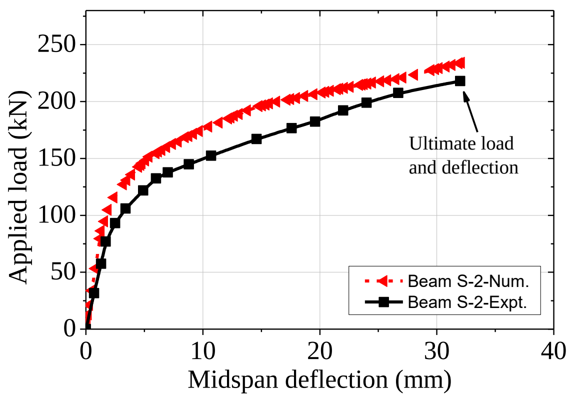

(b) PSB with steel tendons (Jiang et al. [21])

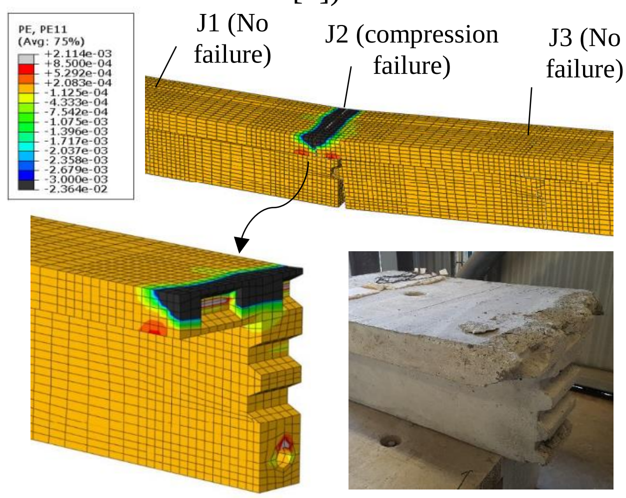

(c) Failure mode of Beam BS1

Fig. 4. Numerical vs experiment results

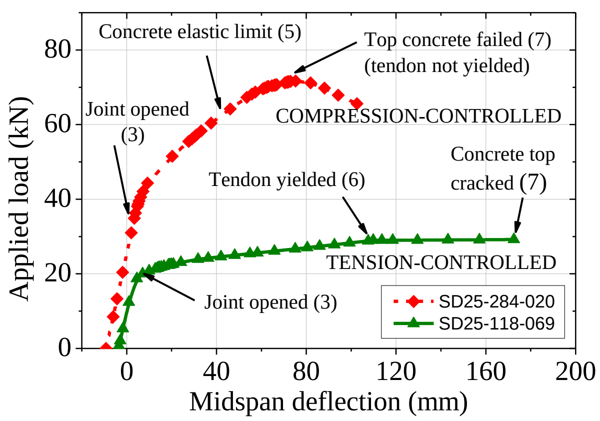

(a) Simulation

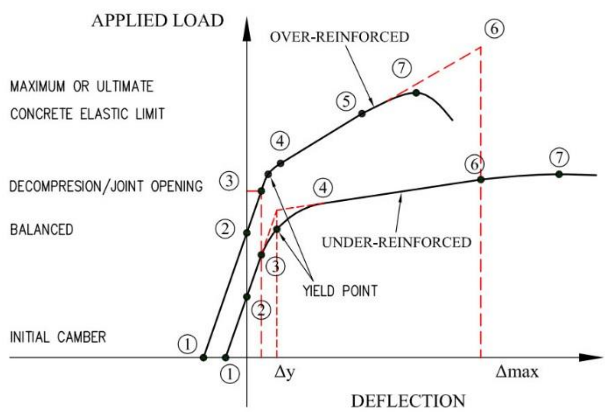

(b) Generalized responses

Fig. 5. Load-deflection curves

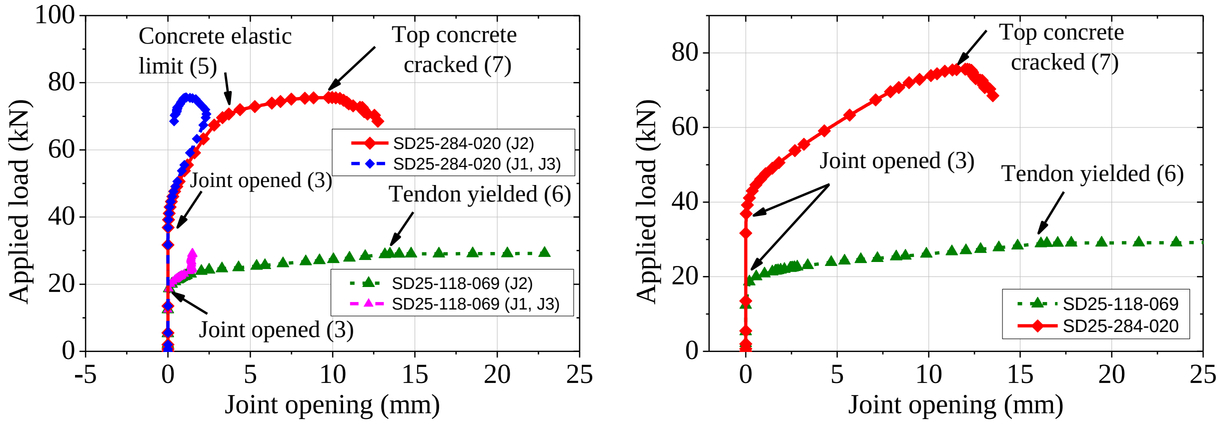

(a) each joint (b) total opening

Fig. 6. Load vs joint opening curves (refer to Fig. 2 for joints' locations)

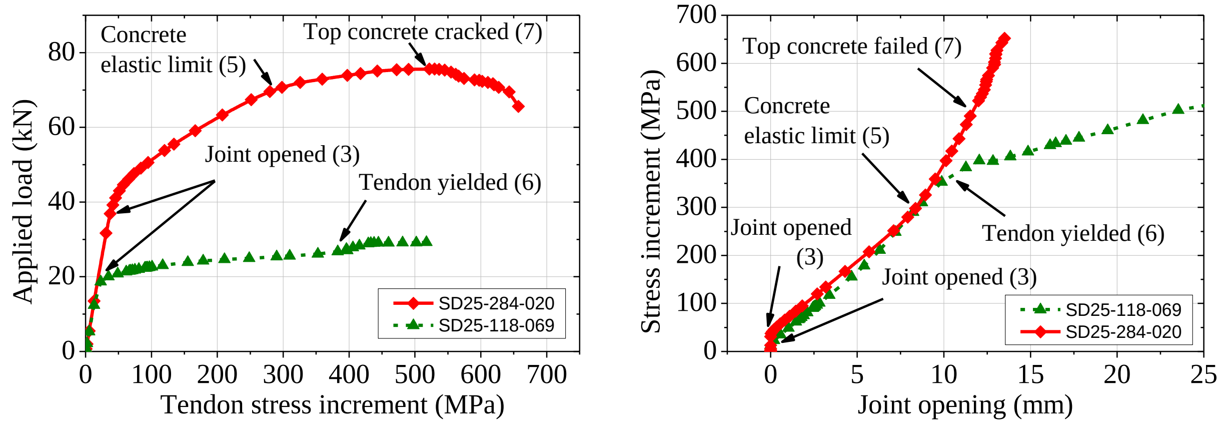

(a) Load vs stress increment (b) Stress increment vs total opening

Fig. 7. Relations between applied load, stress increment and joint opening

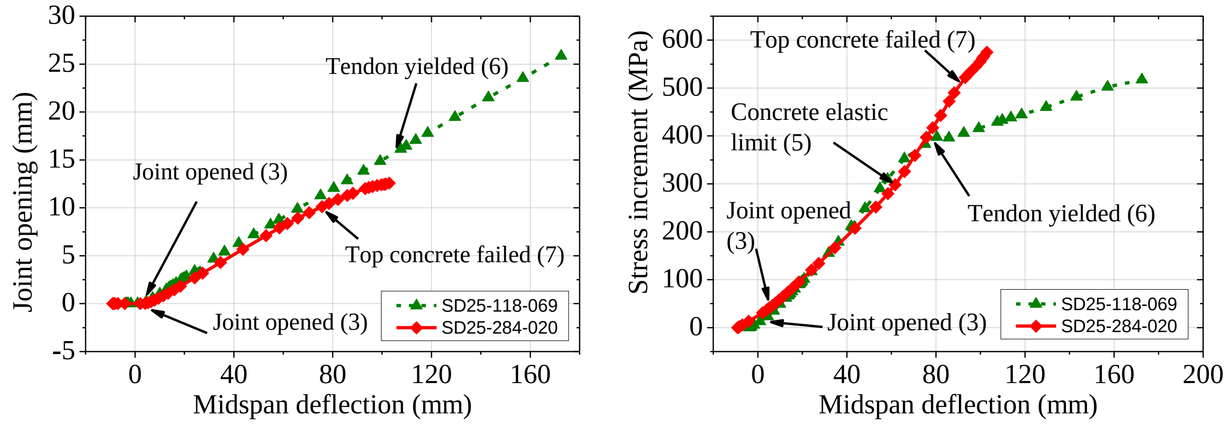

(a) Joint opening vs midspan deflection (b) Stress increment vs midspan deflection

Fig. 8. Relations between joint opening, deflection and stress increment

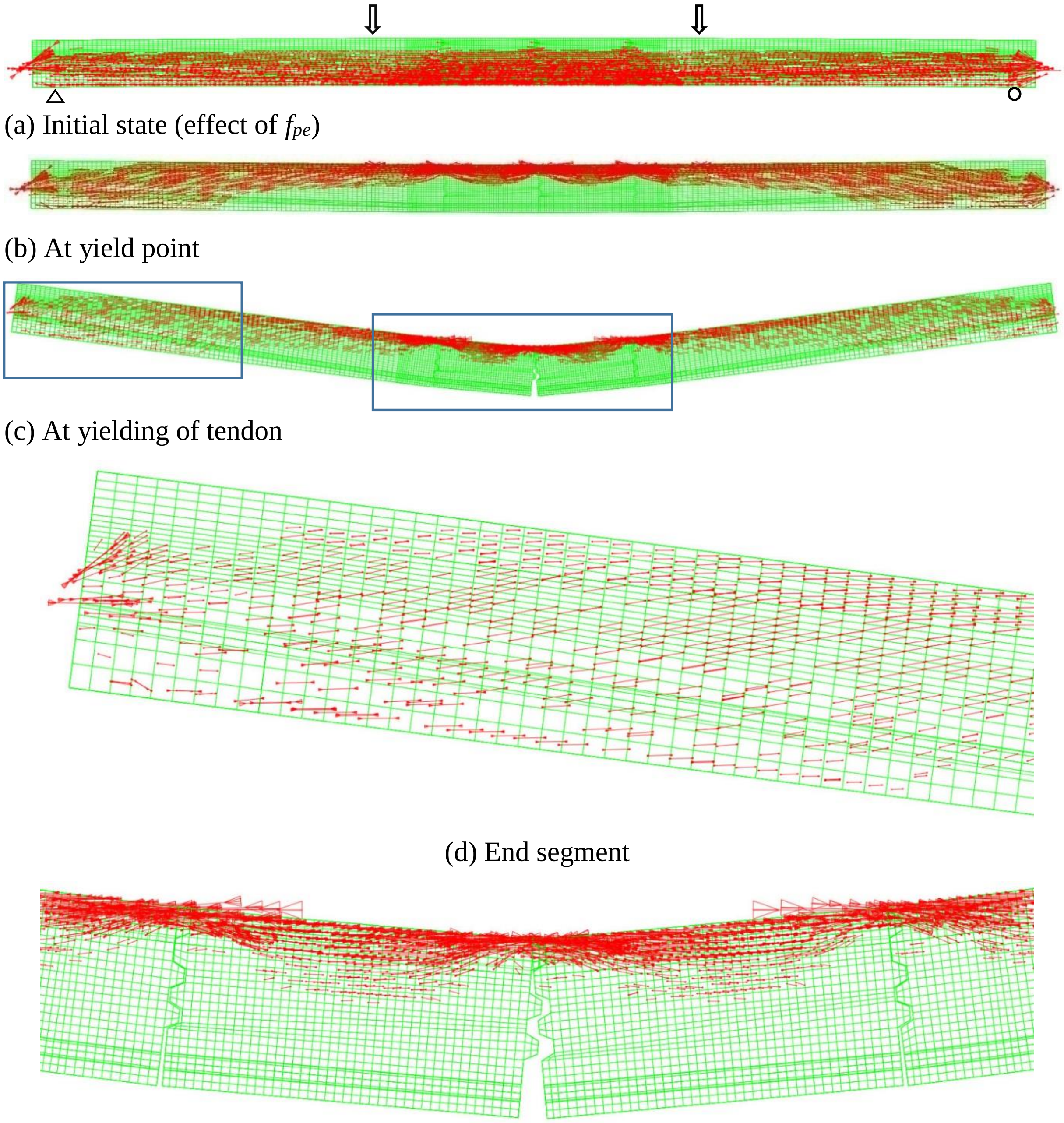

(a) Initial state (effect of f_{pe})

(b) At yield point

(c) At yielding of tendon

(d) End segment

(e) Central segments

Fig. 9. Beam SD25-118-069: principal compressive stress distributions

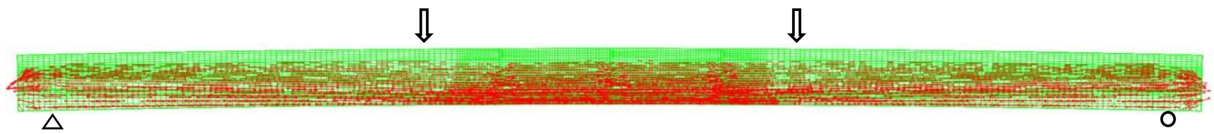

(a) Initial state (effect of f_{pe})

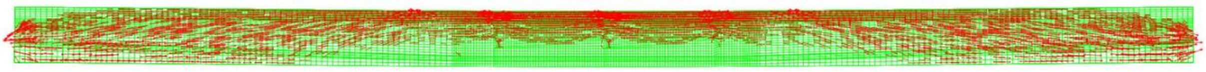

(b) At yield point

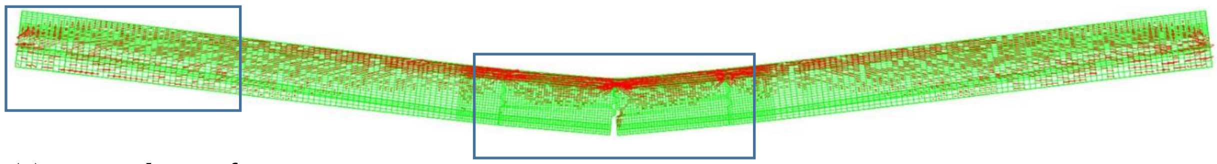

(c) At crushing of concrete in compression zone

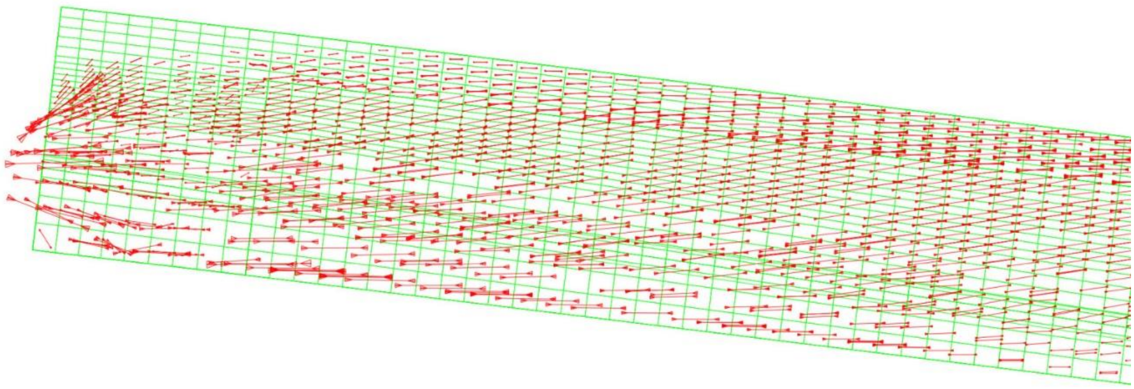

(d) End segment

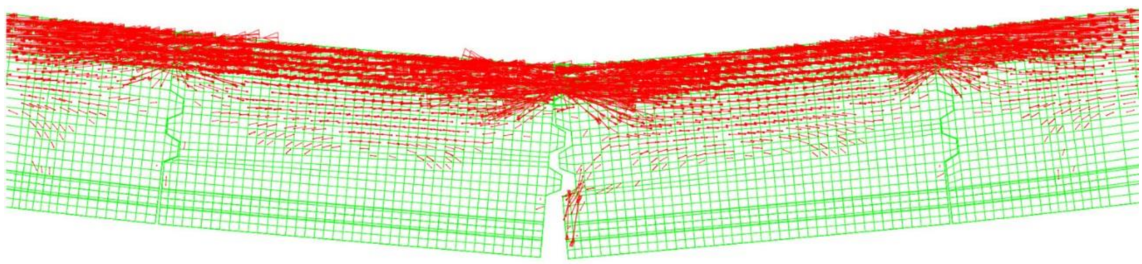

(e) Central segments

Fig. 10. Beam SD25-284-020: principal compressive stress distributions

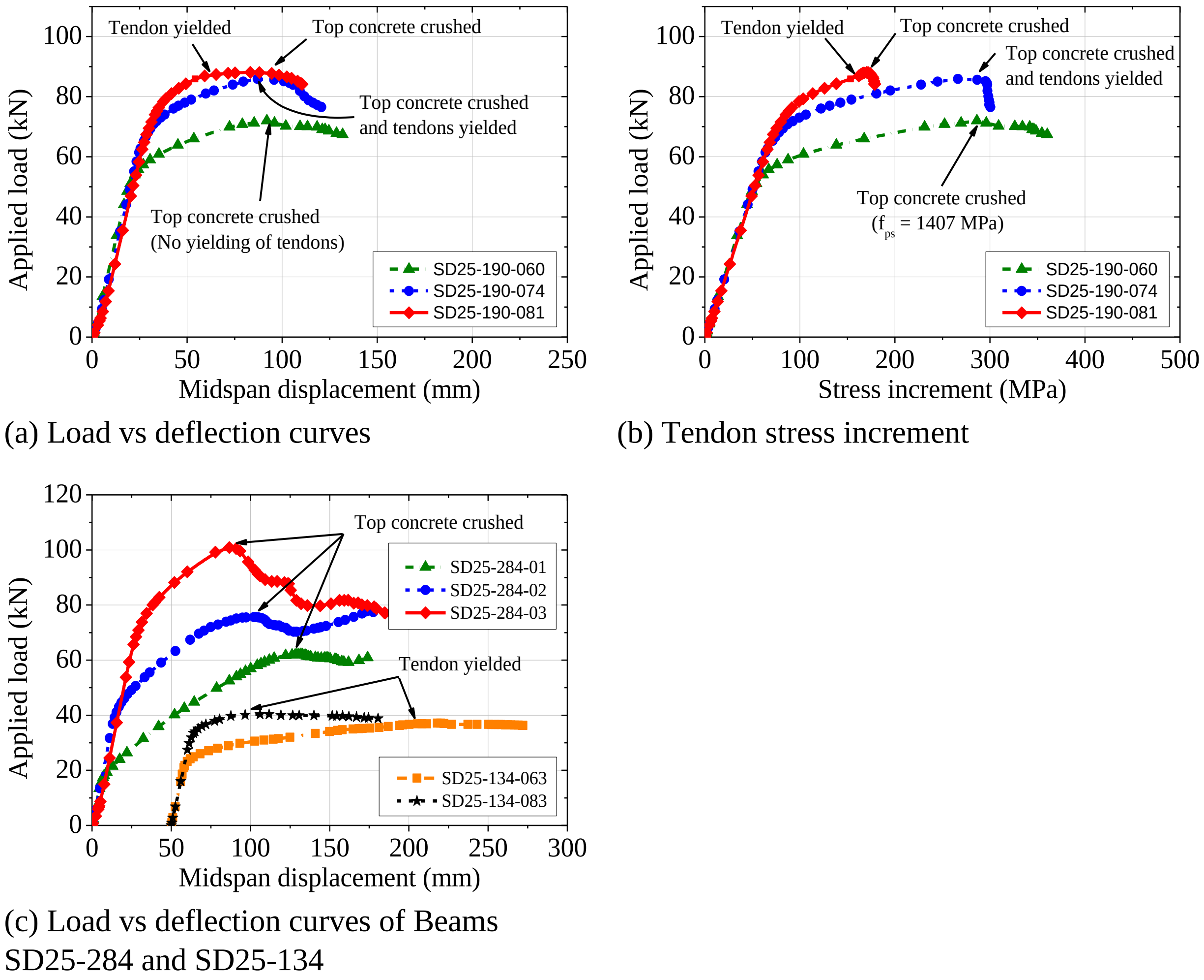

(a) Load vs deflection curves

(b) Tendon stress increment

(c) Load vs deflection curves of Beams SD25-284 and SD25-134

Fig. 11. Effect of f_{pe}

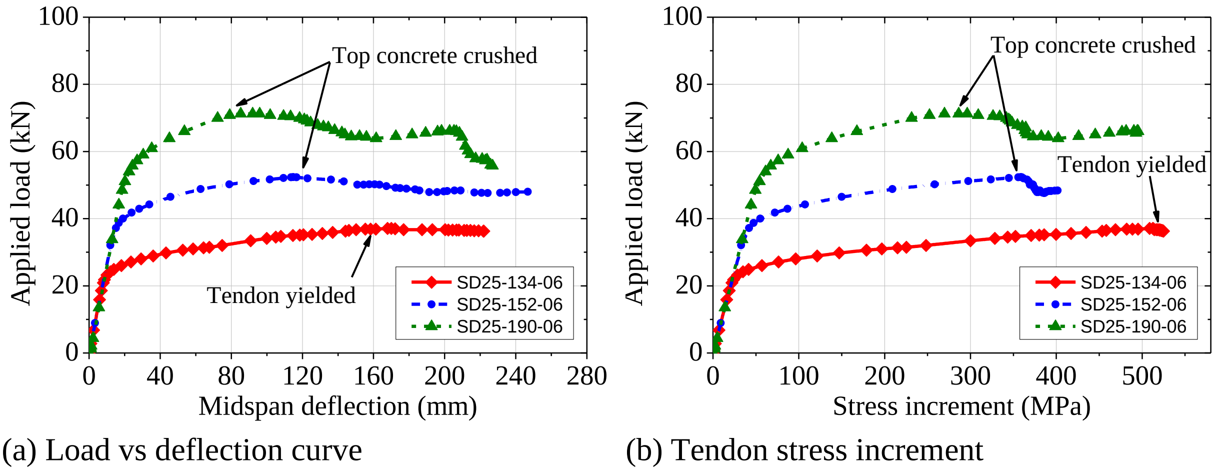

(a) Load vs deflection curve

(b) Tendon stress increment

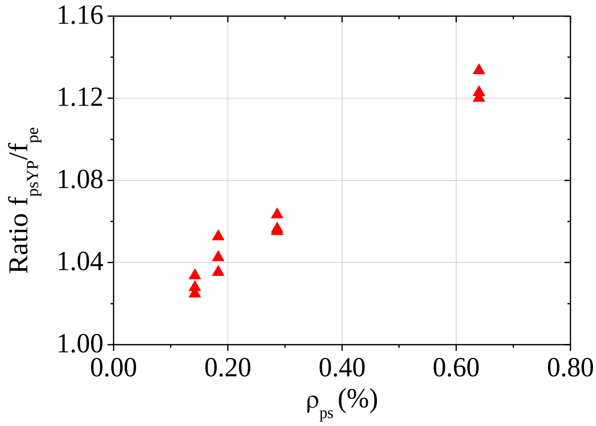

(c) stress increment at yield point

Fig. 12. Effect of A_{ps}

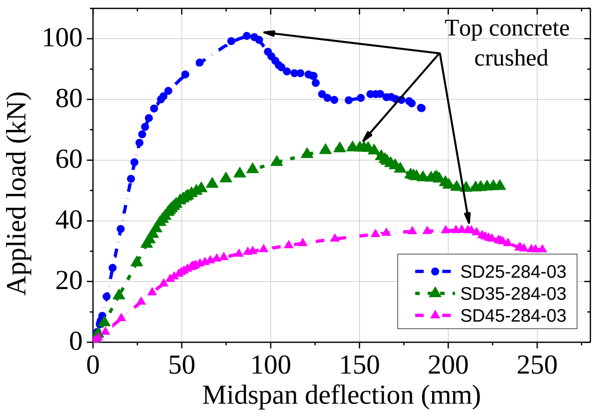

(a) Load vs deflection curve

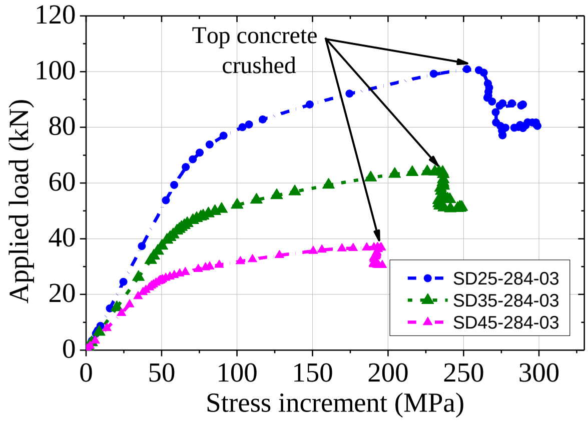

(b) Tendon stress increment

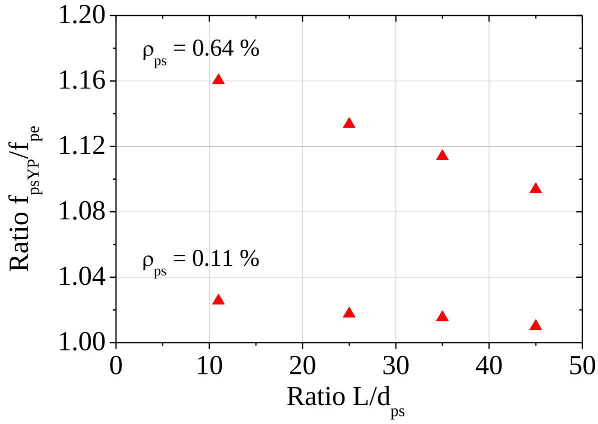

(c) tendon stress at yield point

Fig. 13. Effect of L/d_{ps}

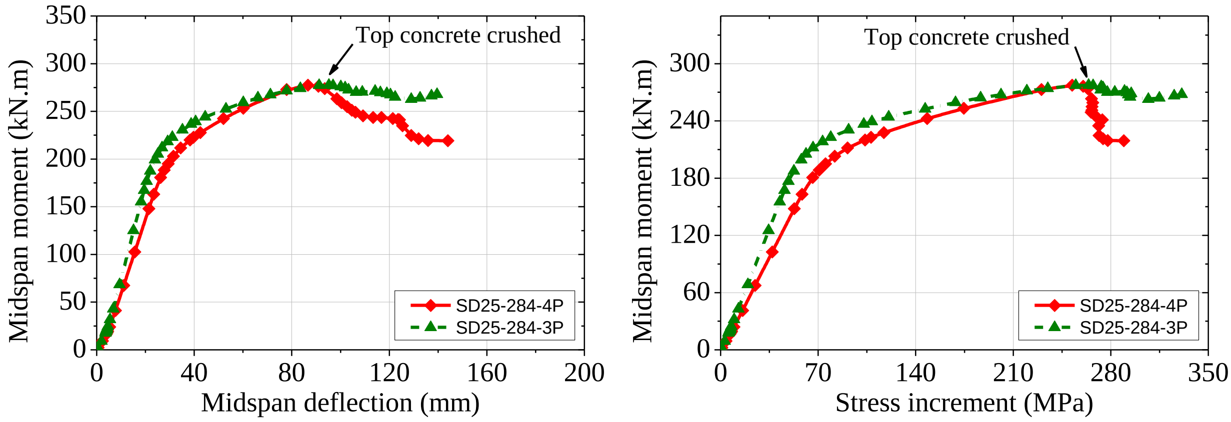

(a) Load vs deflection curve (b) Tendon stress increment

Fig. 14. Effect of load type

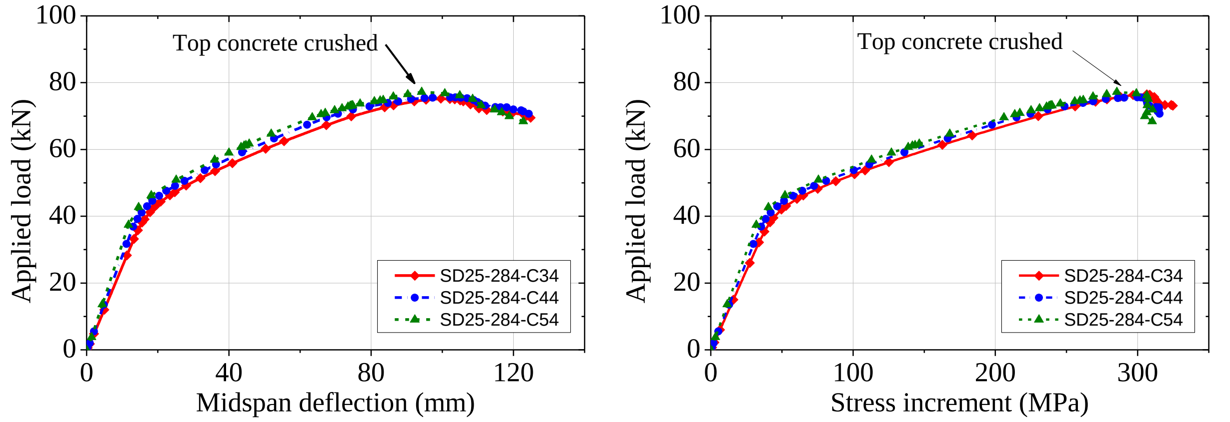

(a) Load vs deflection curve (b) Tendon stress increment

Fig. 15. Effect of f'_c

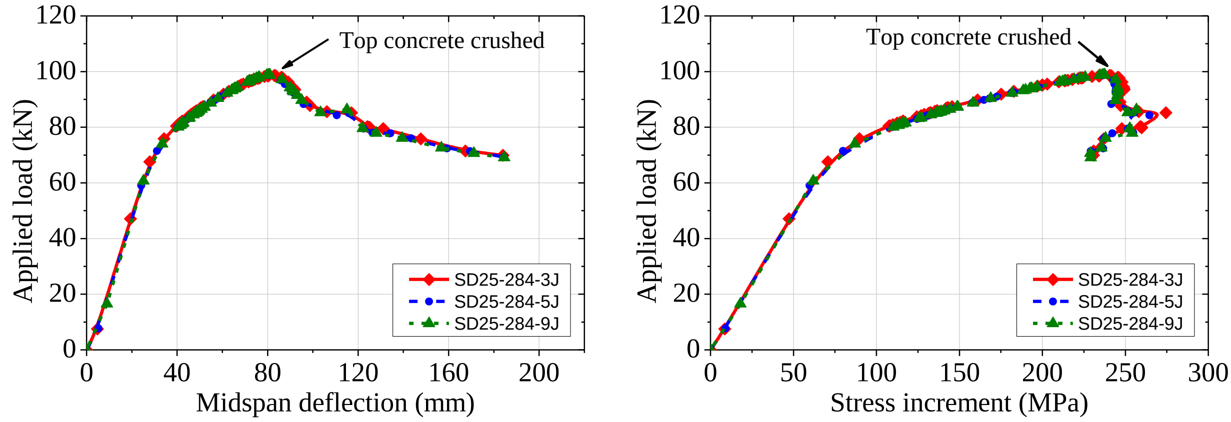

(a) Load vs deflection curve (b) Tendon stress increment

Fig. 16. Effect of number of joints

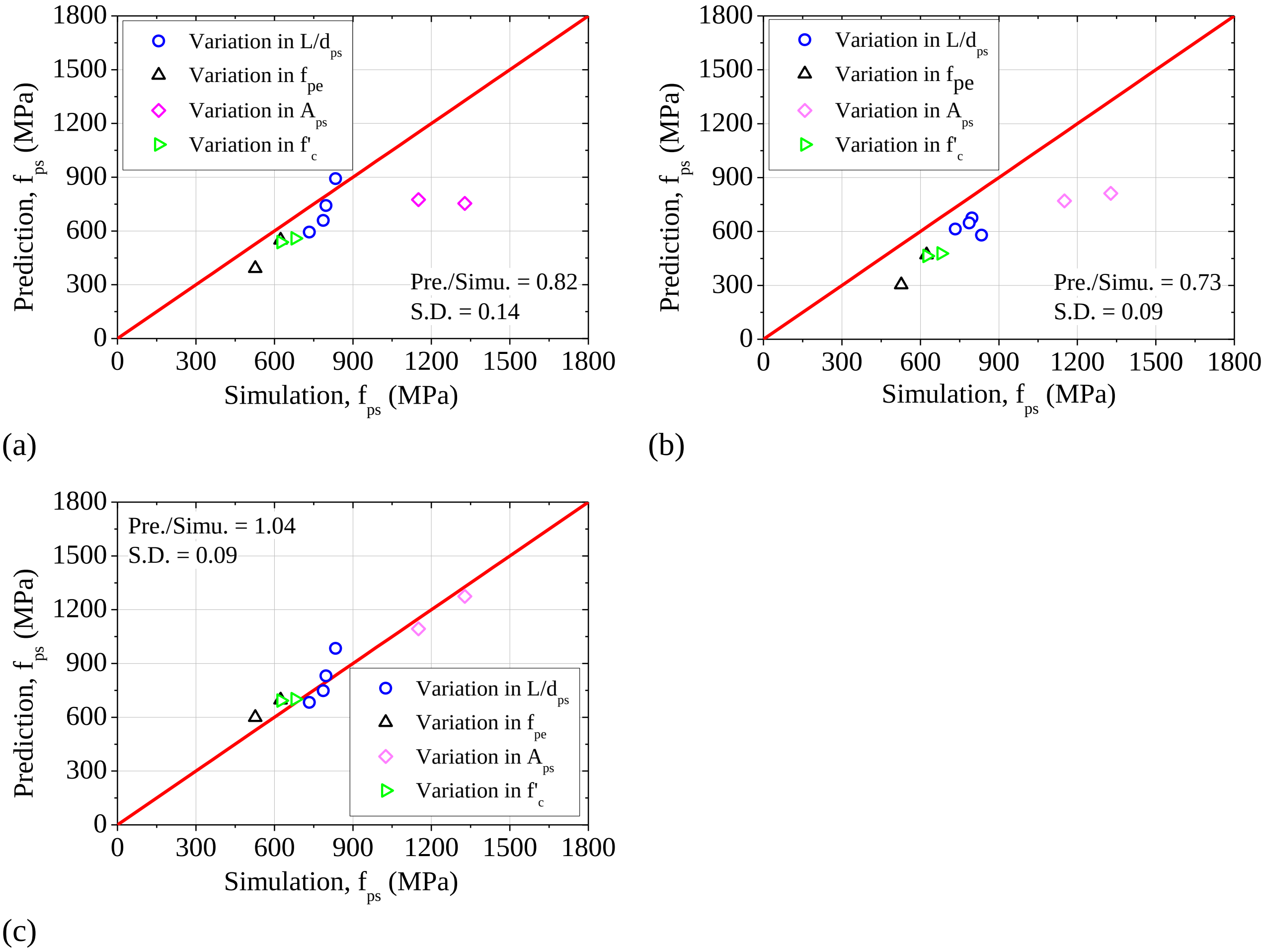

Fig. 17. Prediction of f_{ps} by: a) AASHTO LRFD [40]; (b) ACI 318 [41]; (c) Naaman and Alkhairi [42]

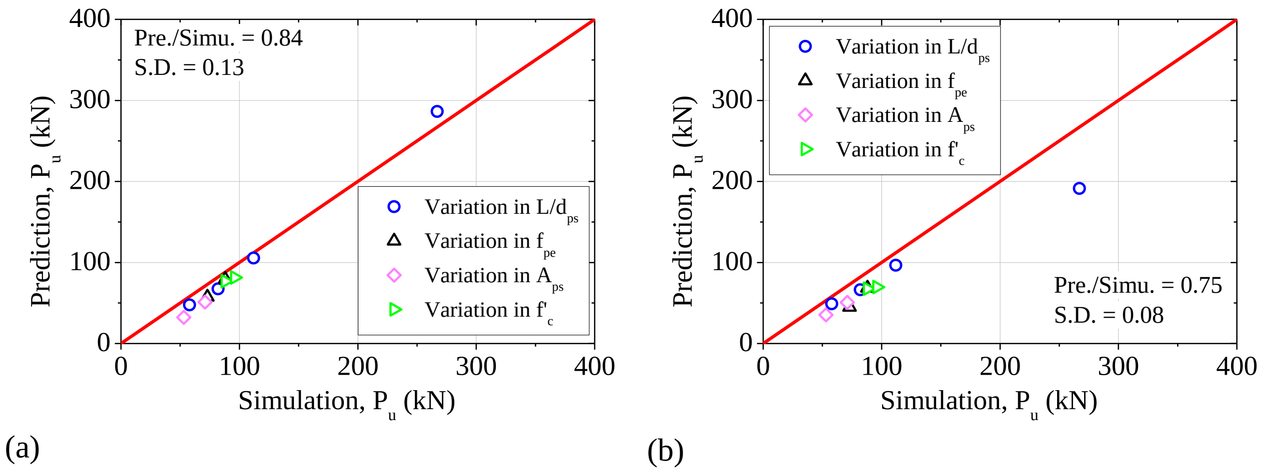

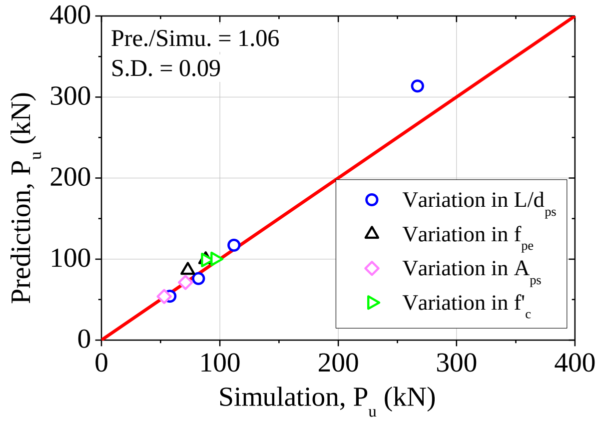

(c)

Fig. 18. Prediction of P_u by: a) AASHTO LRFD [40]; (b) ACI 318 [41]; (c) Naaman and Alkhairi [42]

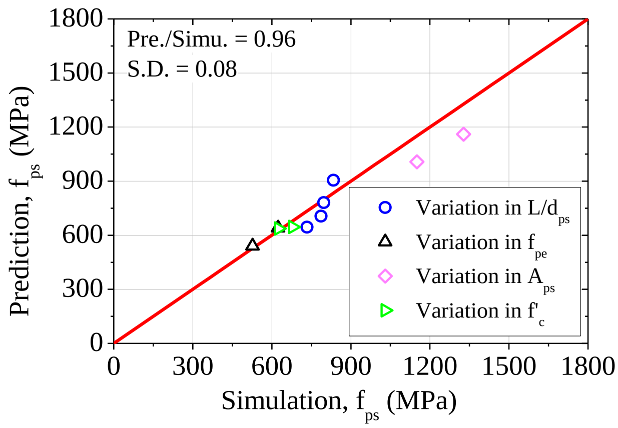

(a)

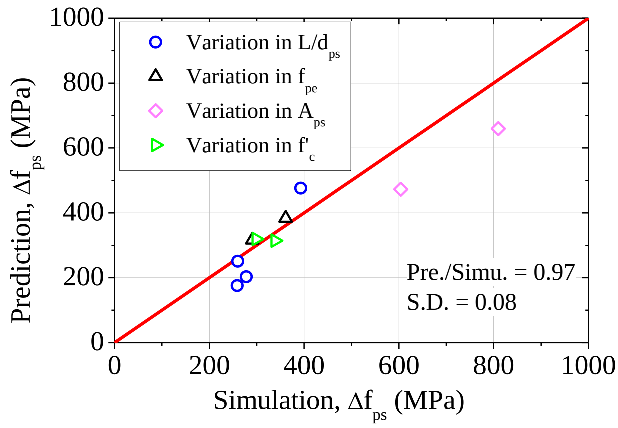

(b)

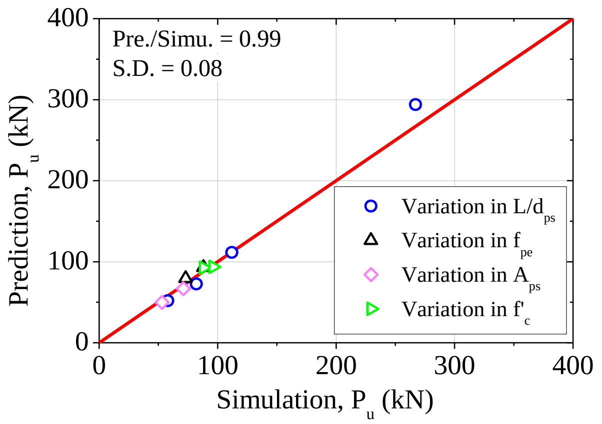

(c)

Fig. 19. Performance of modified Naaman and Alkhairi [42]'s model for the prediction of: (a) f_{ps}; (b) Δf_{ps}; (c) P_u